Weiping Lei

A comparison of the deep structure of the Mid-Norwegian margin and the South China Sea

Master's thesis in Petroleum Geology
Supervisor: Per Terje Osmundsen
November 2020

Master's thesis

NTNU
Norwegian University of Science and Technology
Faculty of Engineering
Department of Geoscience and Petroleum

NTNU
Norwegian University of
Science and Technology

Weiping Lei

A comparison of the deep structure of the Mid-Norwegian margin and the South China Sea

Master's thesis in Petroleum Geology
Supervisor: Per Terje Osmundsen
November 2020

Norwegian University of Science and Technology
Faculty of Engineering
Department of Geoscience and Petroleum

■ NTNU
Norwegian University of
Science and Technology

Abstract

Rifted basins are now an important type of basin that produces petroleum, especially in Atlantic margin. The study of rifting process is important for the petroleum prospecting. In this study, we focus on the Mid-Norwegian margin with the emphasis on the Møre and Vøring basin. These two basins have a long extension history after the Caledonian orogeny. The extension history can be divided into 3 main stages: Permian to Triassic, the Late Jurassic to the Early Cretaceous and the Late Cretaceous to Early Tertiary. These rifting periods are not continuous, resulting in 3 unconformities in the study area. In these three unconformities, the Base Cretaceous Unconformity is the most widely recorded in the Mid-Norwegian Margin. Actually, this unconformity represents the ending of the Late Jurassic to the Early Cretaceous rifting phase, tentatively termed as the Base Cretaceous Unconformity. In the study area, the depth of this reflector varies from less than 5 km in the drilled area to 15 km in the deep basin, which indicates different degrees of extension caused by the normal faults. Similarly, the undulation of the top basement is also very notable. Below the top basement, we also recognized some intra-basement reflectors and provided some possible interpretations.

Based on the new terminology of domains and breakaway complexes, we subdivided the study area in terms of margin domains and classified major faults in terms of breakaway complexes. Most of the seismic reflection lines used in this study contain necking and distal domain, these two domains are bounded by the outer necking breakaway complex, which is considered as a typical structure in Mid-Norwegian margin. It creates a dramatical accommodation increase in its hanging wall and cuts into the lower crust and upper mantle, coupling the deformation from upper crust to upper mantle. In the distal domain, a distinct feature is the distal breakaway complex, which is the inner boundary of an area of potential tectonic unroofing. Based on this fault, the distal domain can be subdivided into hyperextended and unroofed/exhumed subdomain. In some profiles, this breakaway complex can be clearly observed, giving a strong evidence for possible mantle exhumation.

Since 1990s, South China Sea has been considered as a mini Atlantic, because these two are both born in a divergent geological setting. From two sections across the Eastern subbasin and Southwestern subbasin, we find some differences between the South China Sea and East Greenland-mid-Norwegian conjugate margins. First, two sag basins, Xisha Trough and Baiyun Sag, are notable in the proximal domain. In these two sag basins, some normal faults are interpreted to incise into the mantle rocks, and they are widely considered as failed continental breakup, possibly resulting from a disappearance of geothermal source. The outer necking breakaway complex, so typical in the Mid-Norwegian margin, cannot be found in South China Sea. There, the necking domain seems to connect with the distal domain directly and the boundary of these two domains is ambiguous. The distal domain of South China Sea is very narrow and tectonic unroofing caused by low angle detachment faults has not been widely observed. We suggest that South China Sea may not have experienced exhumation or even a hyperextension stage except in two sag basins. These differences may result from different nature of lithosphere, duration of rifting and movement of related plates.

Preface

This thesis is my final assignment for the Master of Petroleum Geology degree at the Norges Teknisk-Naturvitenskapelige Universitet (NTNU).

First, I would like to thank my supervisor Per Terje Osmundsen for guidance, advice and comments. I would have liked to improve my background in tectonics and basin analysis, and due to the outbreak of COVID-19, I was trapped in China and couldn't follow the basin analysis course. I feel so regretful about it. Thank my supervisor Per Terje Osmundsen again for helping me make a great improvement in the thesis studying area.

Secondly, I want to thank Gwenn Peron-Pinvidic that she and Per Terje Osmundsen reminded me of the importance of rheology in basin analysis. Even though I am still weak in this area, I will try to compensate it in the future study and work.

I want to thank Schlumberger for providing Petrel for my interpretation work.

I also want to acknowledge the NTNU- NPD-SCHLUMBERGER PETREL READY Database for the seismic and well data used in this thesis.

I want to thank to Norway and NTNU for giving me a master opportunity, especially without tuition fee, which is really important for developing country students. That is really "Education for a better world".

Finally, I want to thank to myself, the one who made the choice to apply an oversea master program against all opposite opinions 3 years ago.

Table of Contents

List of Figures

List of Tables

1 Introduction

1.1 Purpose of Work

The Mid-Norway margin and South China Sea are typical examples of rifted margins. In this thesis, 11 long seismic profiles will be interpreted from the Mid-Norway margin and compared with representative published interpretation sections from South China Sea to identify and discuss the similarities and differences in large-scale structural framework and basin configuration. In the seismic interpretation, important horizons including but not limited to base Tertiary, base Cretaceous unconformity, seismic basement facies and main fault structures as a basis for subdivision into margin domains and for the classification of faults into breakaway complexes. As the representative sections, including VMT95-004, VMT95-006, VMT95-007 and VMT95-0008, will be converted into depth with the velocity model published by Mjelde et al. (2009) to discuss the depth to the top basement and the position of Moho. Finally, the interpreted sections will be compared to representative, published seismic transects from the South China Sea as a basis for a discussion of the structural and basin architecture of both margins.

1.2 Location of Study Area

The study area includes parts of the Møre and Vøring margins and is situated approximately at latitude 61°-67°N and longitude 1°-7°E. This area is bounded by Møre-Trøndelag Fault Complex in the east, East Shetland basin to the south, Møre and Vøring marginal highs in the west and Vøring basin in the north. The area also includes some notable structural elements introduced in next chapter, that is, Klakk Fault Complex, Fles Fault Complex, Slettringen Ridge, Halten Terrace, Frøya High, Vigra High, and Grip High.

Figure 1.1: Structure map of target area downloaded from NPD[1] containing the location of all the reflection seismic lines

2 Geological Background

2.1 Geological Settings of Mid-Norwegian Margin

2.1.1 Caledonian Orogeny

Four major compressive events are recognized: Finnmarkian (Late Cambrian), Trondheim (Early Arenig), Taconian (Mid-Late Ordovician) and Scandian (Mid Silurian -Early Devonian) (Robert, 2003). Finnmarkian event is believed to have resulted from oceanward subduction of Baltoscandian margin down to an inferred magmatic arc at least eclogite-facies depths, and then rapid exhumation and emplacement of Finnmarkian nappes subducting onto Baltscandian margin. In the Trondheim event, Baltica had started to rotate away from Siberia and slowly approached Laurentia leading to the gradually closing of Iapetus sea. Taconian event is an accretion tectonothermal event along Laurentian margin. Subduction and accretion, including eclogite generation and ophiolite obduction, occurred along Laurentia margin, far from Baltica. Some of these terranes formed during this period were later detached and retransported onto the nappes covering the Baltoscandian margin in the next event. In the Scandian event, the rise of Caledonide allochthons in Norway and Sweden resulted from an oblique collision between Baltica and Laurentia plates in the Late Silurian to the Early Devonian time including a subduction of Baltoscandian margin of Baltica beneath Laurentia to a depth over 120km (Robert, 2003).
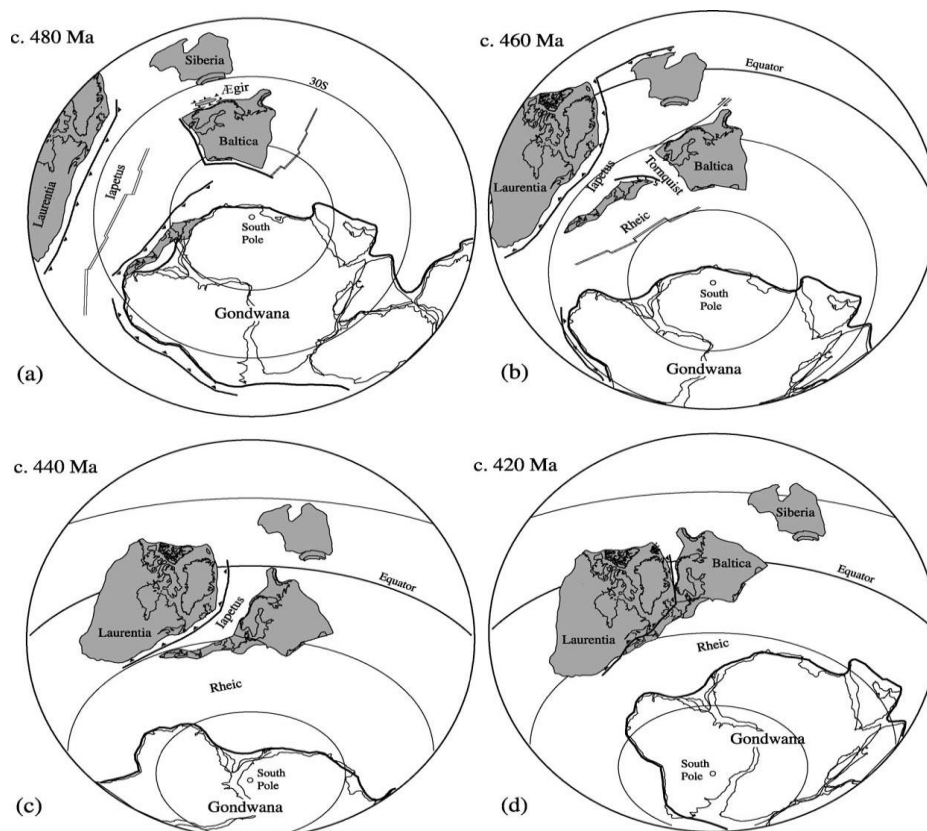
Figure 2.1: Evolution of Laurentia and Baltica plates during Caledonian period (Robert, 2003)

2.1.2 Permian-Triassic

The tectonics activity along the NE Atlantic margin is frequent in this period. Most continents were assembled in the supercontinent Pangea. The Pangea appears to have been inherently unstable, leading to the beginning of continental rifting. In the region of the future margin, Permian-Triassic basins followed the Caledonian fold belt. In the Late Permian, plenty of sub-basins were formed, caused by slight movement along some intra-basinal faults. This tectonic event is considered as the initial rift phase. In Triassic, this area experienced 4 sedimentary phases. The first is an Early Triassic syn-rift phase when the dominantly marine sediment infill pattern was controlled by continued fault-block rotation and tectonic activity along several structural lineaments. The second is middle Triassic inter-rift phase when a continental depositional environment was established resulting from a relative decrease in the rate accommodation. The third is a Late Triassic inter-rift phase. In this period, the forming of thick evaporite in isolated marine sub-basins was triggered by an arid climate, oscillation in the relative sea level and possibly, the establishment of a structural threshold to the Borealic open marine seaway. The last is a later Late Triassic inter-rift phase representing the establishment of a fluviolacustrine depositional environment (Müller et al., 2005).
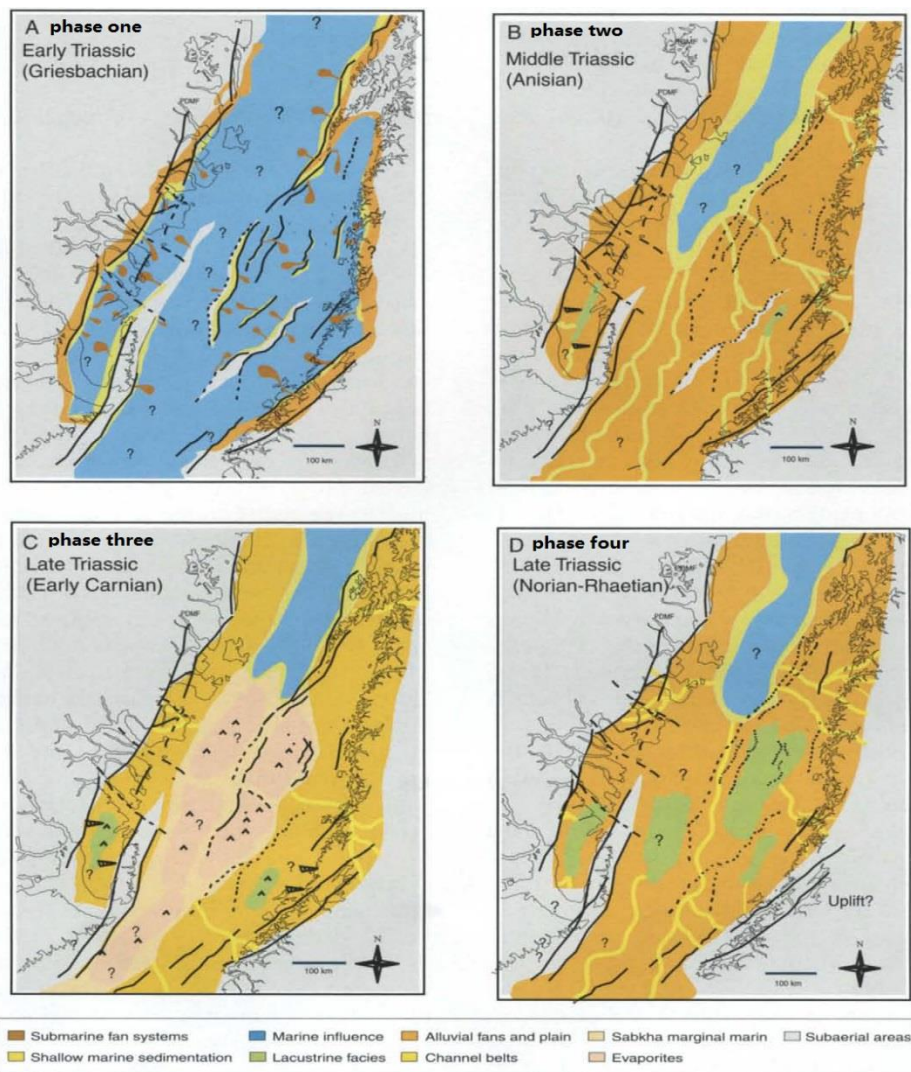
Figure 2.2: Paleogeographic map showing sediment system of the East Greenland-Mid-Norwegian region in the Triassic (Müller et al., 2005)

2.1.3 Late Jurassic to Early Cretaceous

In the Triassic-Jurassic, a change to rift tectonics related to early seafloor spreading in the Tethys to the southeast and in the proto-central Atlantic to the southwest occurred in the North Atlantic transition zone (Doré et al. 1999). Seafloor spreading in the Central Atlantic began in the Early Middle Jurassic and Early Jurassic rifting is considered to have taken place in the sea of the Hebrides Basin (Morton, 1989) and some extensional fault activities in this stage are documented as far northeast as offshore mid-Norway (Blystad et al. 1995).

The most intense phase of rifting happened in the latest Middle to the Late Jurassic times, with a varying time based between basins or intra-basinal provinces. An approximately E-W least principal stress direction was regionally prevalent, as exemplified by the consistent close-to-northerly trend of the unequivocal Jurassic rift basins (shown in Figure 2.3a): Halten Terrace, Viking Graben, East Greenland rift and Porcupine Basin. These N-S striking basins can be exactly described as Jurassic rifts bordering the NE Atlantic margin (Doré et al. 1997b). Færseth et al. (1995) proposed that this E-W extension may have been inherited from an earlier (Permian-Triassic) extensional period.
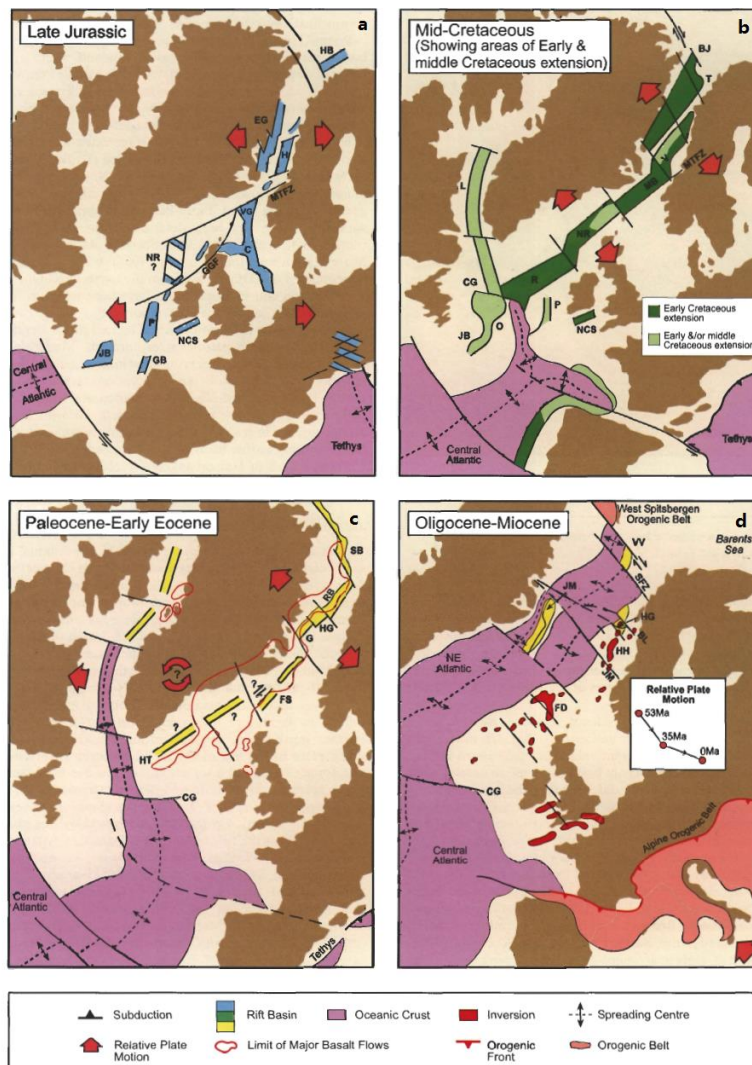
Figure 2.3: Plate reconstruction including Late Jurassic, mid-Cretaceous, Paleocene and mid-Cenozoic (Doré et al. 1999)

In the Early Cretaceous, the seafloor spreading of Tethyan had ceased and was replaced by subduction on the northern margin of the ocean. Atlantic spreading propagated northwards and by the Aptian times oceanic crust was established between the North Iberian margin and the Grand Banks (Driscoll et al., 1995). And the N-S Tethyan rift propagation direction is switched to NE-SW trending rifts. A series of NE-SW faults in this period bounding the Magnus and Manet highs and Margareta Spur specifically describe the southeastern margin of Møre Basin (Reynir Fjalar Reynisson, 2010).

A large amount of tectonic and stratigraphic structures in the Vøring Basin observed by Lundin & Doré (1997) indicate an extensional tectonic event of the Mid-Cretaceous age, which is seen on seismic data as a mild to angular unconformity in outer Vøring Basin, Træna Basin and Ribban Basin.

2.1.4 Late Cretaceous to Early Tertiary

Lundin & Doré (1997) proposed that the Latest Cretaceous-Early Tertiary rifting appears to have started in the Late Maastrichtian, while break-up occurred in the Early-Eocene. Møre Basin margin also broke up in the Early Tertiary, but there are few signs of preceding brittle faulting of margin. Only in the outermost part of basin some Tertiary faulting can be documented (sawn in VMT95-008). Isopach maps show that the Palaeocene section thickens westwards until masked by the Early Tertiary lava, suggesting an increase in lithospheric thinning toward basin margin (Reynisson et al., 2010).

2.1.5 Paleogene

During plate separation in the Early Eocene, a reversal of horizontal stress patterns took place whereby NW-SE extension gave way to SE-directed compression, attributable to ridge push forces from the adjacent ocean. As would be expected, in situ stress measurements show that this NW-SE compressive regime still exists at present in much of NW Europe. The stress pattern is also consistent with the relative motion of Europe and Africa, and hence with Alpine closure. New compressive regime gave rise to widely distributed inversion structures along Atlantic margin. The most commonly observed inversion features are elongate domes which, although only gently deformed, are aerially and vertically extensive (Doré et al. 1999).

Most of structures show evidence of multiphase inversion. The timing of activity on Norwegian Sea structures has been described by Dore & Lundin (1996) but has since been refined by detailed examination of 3D seismic data. Ormen Lange Dome, at the Møre-Vøring transition, underwent its most significant period of deformation in the Late Eocene-Early Oligocene. These observations suggest a systematic younging of inversion northwards (Doré et al. 1999).

Plate reorganization of the Oligocene-Miocene age also gave rise to local renewed extension of North Atlantic margin. Rifting propagated from south to north between Jan Mayen Block and SE Greenland, counterbalancing the fan-shaped spreading (widening northwards) along Aegir Ridge. The extension culminated in the separation of Jan Mayen microcontinent along Kolbeinsey spreading ridge (shown in Figure 2.4), and extinction of Aegir Ridge, at chron 7 time (25 Ma, Oligocene- Miocene boundary) (Doré et al. 1999).

Extension on Norwegian margin may represent a failed attempt at splitting off a microcontinent similar with Jan Mayen. The relationship between the Cenozoic extension and inversion is not yet clear. As suggested by Dore & Lundin (1996), it is possible that these tectonic effects occurred simultaneously as transtensional and transpressional

elements of a strike-slip regime. Dore et al. (1999) propose, however, that the extension was a discrete event and interrupted a general background of mild compression deriving from ridge-push, as also suggested for East Greenland (Reynisson et al., 2010).
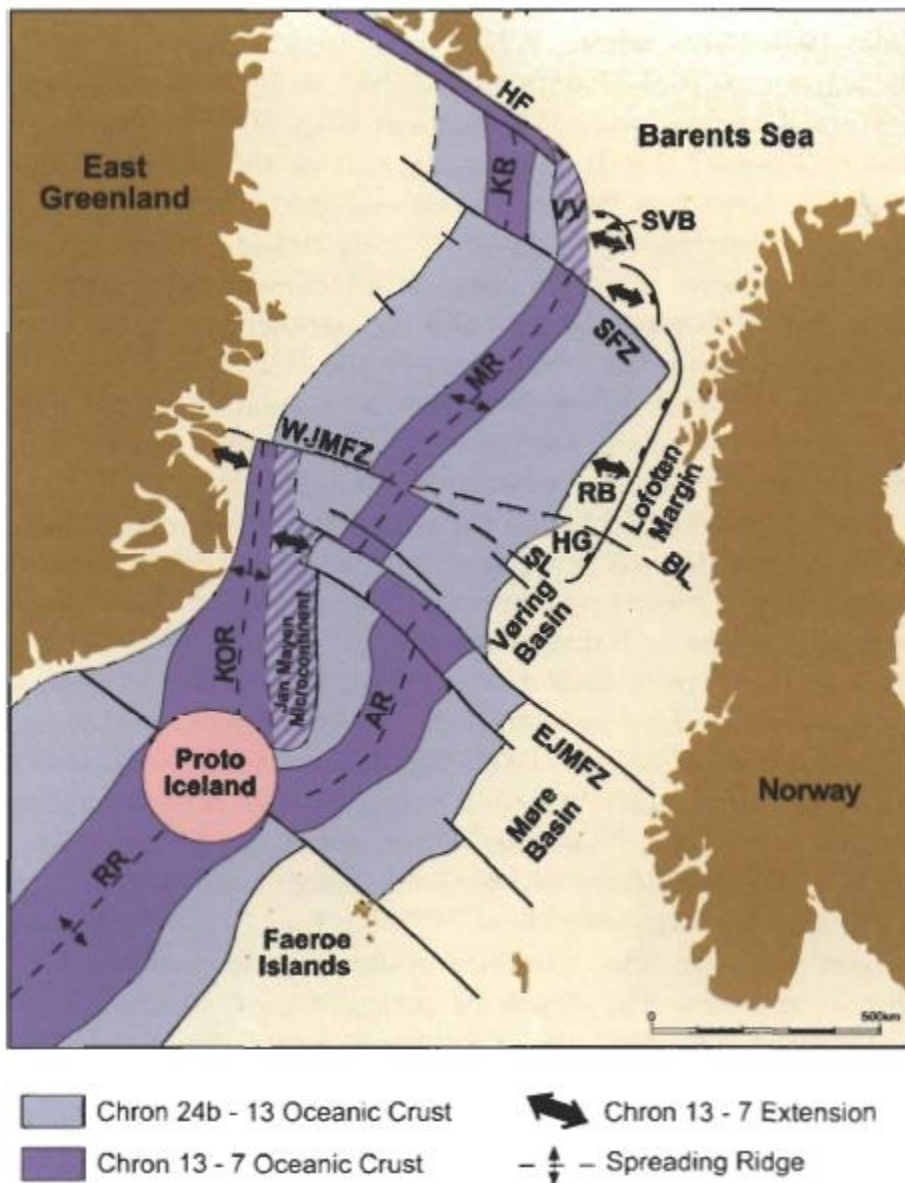
Figure 2.4: Sketch map of a proposed mid-Cenozoic linked extensional system affecting East Greenland, Jan Mayen, the northern Vøring Basin and the western Barents Sea. Plate reconstruction is to chron 7 time (25Ma) (Doré et al. 1999)

2.1.6 Neogene Uplift and Erosin

The last major tectonic phase on Atlantic margin, regional uplift of the Neogene age (Figure 2.5), was arguably one of the most important, not least because it shaped the distribution of sea and landmasses we see today (Dore et al. 1999). A major sedimentary wedge of Pliocene age progrades away from the mainland and is itself truncated by the unconformity at the base of the Quaternary. This pattern is consistent around most of Norwegian mainland, which is ringed by concentric subcrops indicating domal uplift and late emergence (Dore et al. 1999).
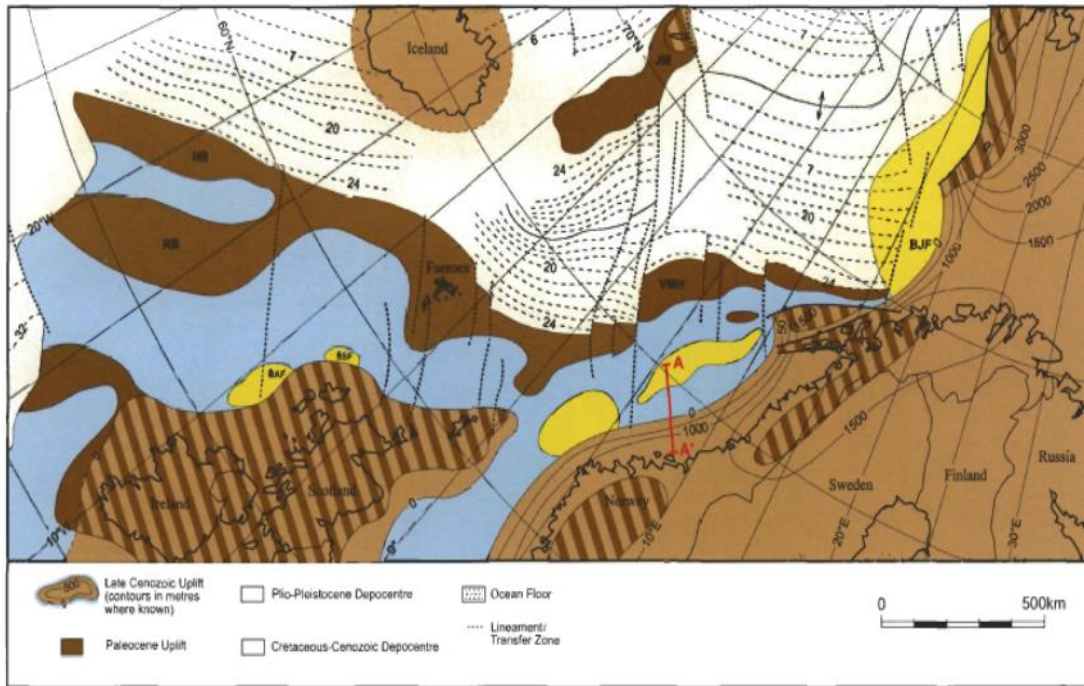
Figure 2.5: Map showing Cenozoic uplift along the northwest European Atlantic margin (Doré et al. 1999)

The domes and arches controlled the sedimentation on Vøring margin in the post-Middle Miocene times when the Late Miocene muds and oozes filled in and buried the existing relief. Sedimentation continued into the Pliocene interspersed with ice-rafted debris signifying regional cooling and formation of mountain glaciers (Reynisson et al., 2010).

The morphology of Fennoscandia and the almost complete absence of onshore Mesozoic and Cenozoic sediments have for more than a century been interpreted in terms of epeirogeny uplift. In particularly, a Lower to Middle Miocene hiatus on Norwegian shelf may be related to renewed tectonic uplift of the eroded landmass in the Late Oligocene or the Early Miocene time, later amplified by the isostatic response to the numerous glaciers and inter-glaciers since the Late Pliocene. This induced large-scale glacial erosion of shelf and mainland sourcing the voluminous wedges of glacial sediments centered near present shelf edge (Reynisson et al., 2010).

2.2 New Model for Passive Margin

Péron-Pinvidic et al. (2013) proposed that many rifted margins are characterized by a certain set of comparable architectural elements and distinct domains would represent the structural fundaments of many rifted margins. These distinct domains are the proximal, necking, distal, outer and oceanic domains (shown in Figure 2.6). Osmundsen & Péron-Pinvidic (2018) proposed a new terminology to describe the structural boundaries that separate rift margin domains. The new terminology introduced by Osmundsen & Péron-Pinvidic (2018) is the breakaway complex, which is used to denote a composite, laterally persistent tectonic boundary that consists of the breakaway zone of several faults that facilitated similar changes in the margin architecture (shown in Figure 2.7e). At the Mid-Norwegian margin, five principle breakaway complexes are defined to separate the proximal, necking, distal, outer and oceanic domains (shown in Figure 2.6).
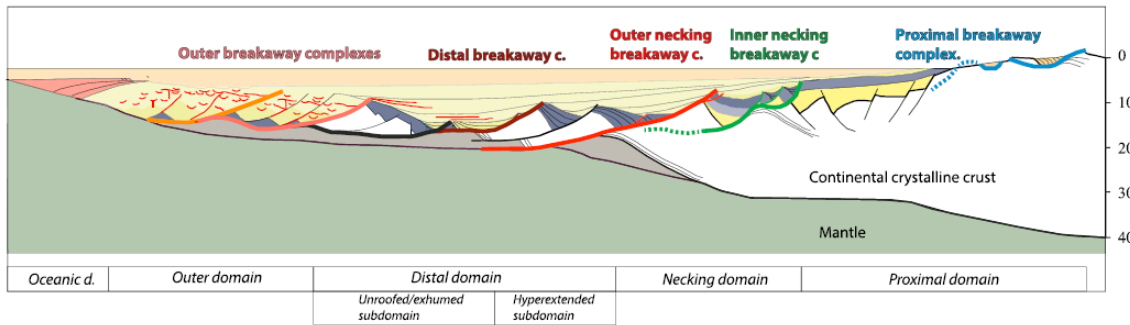
Figure 2.6: Principle 2D sketch of rifted margin showing the configuration of margin domains and domain-bounding breakaway complexes (Osmundsen & Péron-Pinvidic, 2018)

The proximal domain represents the inboard continental crust that has been stretched at low values of extension. In this domain, faults are considered to only affect the brittle upper crust and crust thinning is moderate, resulting in a modest amounts of accommodation space during and after rifting. Proximal breakaway complex is the inner border for the proximal domain, and it defines the border between extended margin and 'unextended' continent and commonly comprises High-β normal faults type 0 shown in Figure 2.7b.

In the necking domain, Moho defines an inflection point associated with a drastic crustal thinning from ~30 to less than 10 km. The Top Basement and Moho converge here, and the necking domain contains an area of the margin characterized by a marked basinwards increase in total accommodation space (Péron-Pinvidic et al., 2013). In this domain, two notable breakaway complexes can be found here: inner necking and outer necking breakaway complex. The inner necking breakaway complex defines the boundary of the slightly stretched proximal domain and more highly extended necking domain. It is normally related to an abrupt but moderate accommodation increase and to a large, basinward-dipping normal fault incising into the ductile middle crust. Conceptually, the inner necking breakaway complex commonly consists of High-β normal faults type 1 shown in Figure 2.7d and faults transitional between Low-β normal faults type 1 and High-β normal faults type 1 shown in Figure 2.7a and 2.7d. The outer necking breakaway complex is normally associated with the first fault that cuts the middle crust and continues into lower crust and upper mantle. The inner boundary for the distal domain will commonly be located at its hanging wall cutoff. Notably, the outer necking breakaway complex is associated with a very large accommodation increase and, conceptually, with the coupling of deformation between the crust and mantle. Erosional sedimentary unconformities are often observed in the necking domain, attesting to a complex uplift/subsidence history related to the associated breakaway complexes. The outer necking breakaway complex comprises a variety of faults including High-β normal faults type 1 shown in Figure 2.7d as well as more planar varieties (Osmundsen & Péron-Pinvidic, 2018).

a. Low-β normal faults, type 1

b. High-β normal faults type 0 (Late to post-orogenic detachment)

c. Low-β normal fault, type 2

d. High-β normal faults, type 1 (coupling detachment)

e. Red color faults constitute the breakaway complex

f. High-β normal faults, type 2 (exhumation detachment)
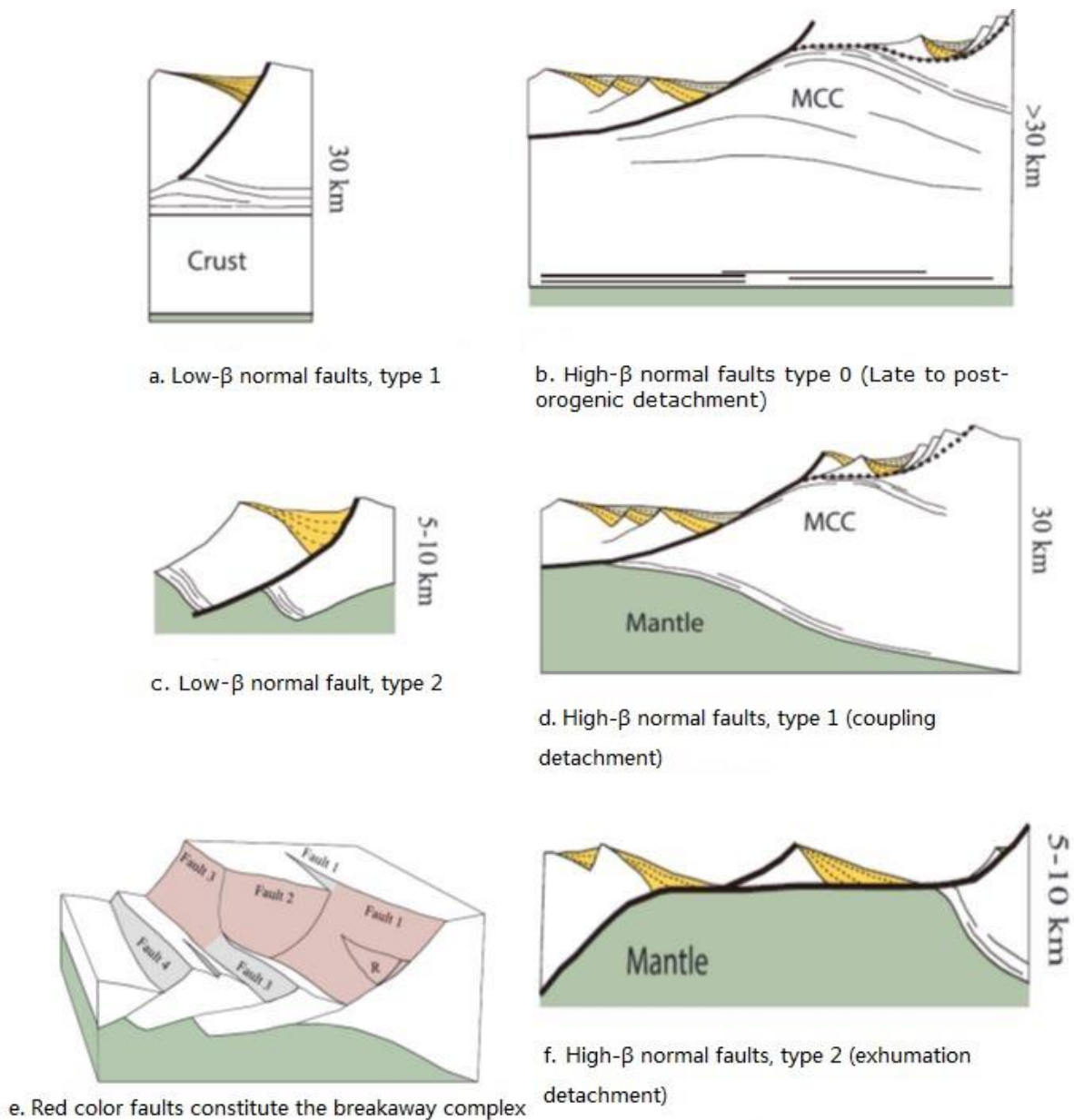
Figure 2.7: Simple Classification of typical normal faults showing in the rifted margin and illustration of the term breakaway complex (Osmundsen & Péron-Pinvidic, 2018)

The distal domain is regularly referenced as the hyperextended domain where some geophysical survey shows that basement has been thinned down to <10 km. Magmatic intrusions and infiltrations are regularly suggested in this domain. The distal breakaway complex in this domain defines the inner boundary for an area of potential major tectonic unroofing and, if extension was sufficient, mantle exhumation. If this happens in successive stages, with one distal detachment fault incising successively into the other, an exhumation breakaway may be defined at the inboard limit for exhumed mantle. Extensional allochthons may often lie on top of the detachment surfaces. The distal breakaway complex consists of High-β normal faults type 2 shown in Figure 2.7f (Osmundsen & Péron-Pinvidic, 2018).

The limits of the outer domain are less well constrained. It is located between the ill-defined basement of the distal domain and unambiguous oceanic crust. In the study area, the outer domain corresponds to the Møre and Vøring Marginal Highs. The outer breakaway complex

is associated with ridge complex in the margin' outer domain, where successive incising faults are interpreted to cut and displace top basement. It also consists of High-β normal faults type 2 shown in Figure 2.7f and can be developed laterally from Low-β normal faults type 2 shown in Figure 2.7c (Osmundsen & Péron-Pinvidic, 2018).

The oceanic domain is bounded by the Continent Ocean Boundary (COB). However, the definition of COB is often ambiguous. This is mainly because either the oceanic crust is accreted very slowly and can be regarded as a heterogeneous basement with unusual geophysical and geochemical characteristics, or because it is masked by material that has blanketing effects on the geophysical signals, such as intrusive or extrusive magmatic rocks or salt, preventing any clear identification (Péron-Pinvidic et al., 2013). The oceanic domain doesn't show in the study area and identification of COB is not included in this work as well.

3 Methodology

3.1 Seismic Data

In this master work, 11 2-D seismic lines, including 8 long parallel seismic lines and 3 transection lines perpendicular to those long lines (location shown in Figure 1.1), have been interpreted to identify structural framework, basin configuration and further to understand the evolution of rifted basin. These seismic lines are obtained from NTNU- NPD-SCHLUMBERGER PETREL READY Database. Some of the lines are not continuous, a narrow gap exists in several lines, including VMT95-002, VMT95-004, VMT95-005, VMT95-006 and VMT95-007. This narrow gap results in the missing of important faults in the interpretation especially in line VMT95-004 and VMT95-005. All lines have been interpreted in time domain and can reach approximate 12s TWT. Time-depth conversion will be performed in line VMT95-004, VMT95-006, VMT95-007 and VMT95-008 with the velocity model from Mjelde et al. (2009). In some terrace, the wells have been drilled to Triassic and well data can be used to identify some horizons above Triassic layer.

For the interpretation, the Schlumberger Petrel software has been used. Petrel is highly commonly used in the petroleum industry as a tool for handling seismic interpretation.

3.1.1 Polarity

Two types of polarity convention are widely used in the world: American polarity and European. In American polarity, positive amplitude represents an increase in impedance, normally displayed in blue. A decrease in impedance yields negative amplitude normally displayed in red. European convention is opposite of American (shown in Figure 3.1.1).
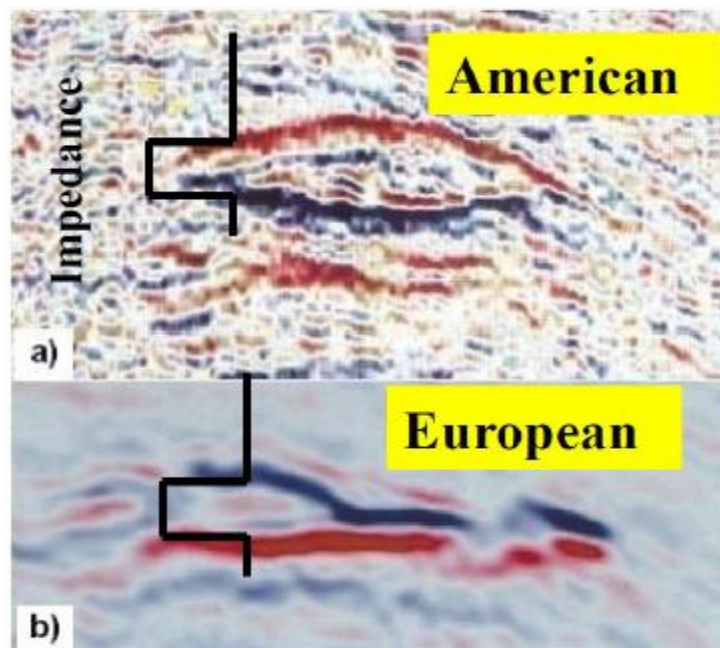
Figure 3.1.1: Top and bottom of a gas reservoir (low impedance zone) in (a) American polarity and (b) European polarity

In marine seismic, sea bottom reflection is a good indicator to determinate the phase and the standard polarity used during the seismic acquisition. In our data, the seismic study shows a peak in the sea bottom reflection (increase of impedance). Base on this (shown in Figure 3.1.2), American standard and minimum phase has been used.
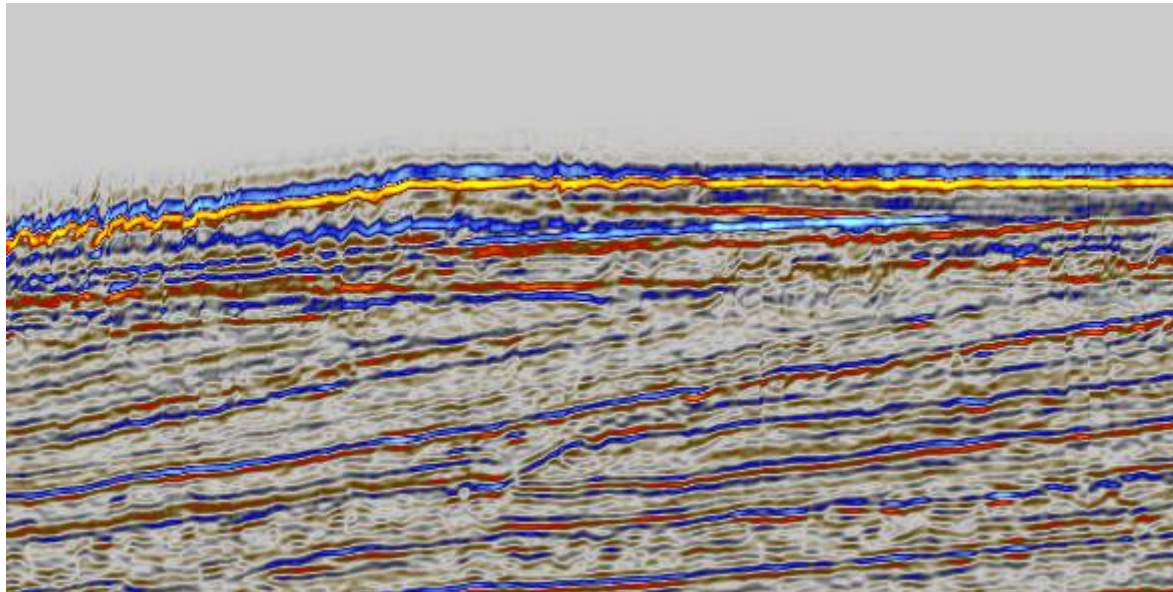
Figure 3.1.2: Sea floor reflection from one of the seismic lines. Blue represents negative amplitude; red represents positive amplitude.

3.1.2 Resolution and Data Quality

The resolution of seismic data controls the level of details visible on the seismic records. The Rayleigh's Limit of Resolution states that two events should be separated by half cycle model. To solve for thickness $\Delta h \geq \lambda/4$, where h represents thickness of the layer and λ represents the wavelength. To resolve for two interfaces that are closely spaced the wavelength is $\lambda/4$. For bed thickness that is less than $\lambda/4$, amplitude and bed thickness become judgmental values. For bed thickness more than $\lambda/4$, the wavelength is used to determine the bed thickness (Kallweit R. & L. Wood, 1982).

The horizontal resolution is decided by the acquisition geometry and Fresnel Zone. According to the ASCII Header, the space between two common mid-points is 12.5m, which is the CMP bin size. The radius of the Fresnel Zone will increase with depth, increased velocity and lower frequency, which will decrease the horizontal resolution.

The data quality is decided by acquisition and can be improved by processing method. Generally, the data quality of these lines varies horizontally and vertically. The shallow part has a better quality, which may result from a higher resolution. Generally, in the western part, data quality in the deep parts of the seismic lines becomes worse than that in the eastern part, which may be caused by the covering of Tertiary lava flow in the west.

3.2 Well Data

Well data can provide the direct evidence for the underground layers. We can pick the selected horizons directly. Especially, in the terrace or structural high area the well can often penetrate into the pre-Cretaceous strata, providing a position for the Base Cretaceous and Base Tertiary and we can pick the horizons based on the well data directly (shown in Figure 3.2). Some wells also contain the zero-phase synthetic data which can give a simple

view to the amplitude and continuity of the selected horizons, such as the well 6406/11/1S shown in Figure 3.2. The well data used in this study are downloaded from NPD[2]. These wells are: 6306/6/1, 6406/11/1S, 6406/8 and 6406/2/1.

Well 6406/11-1S
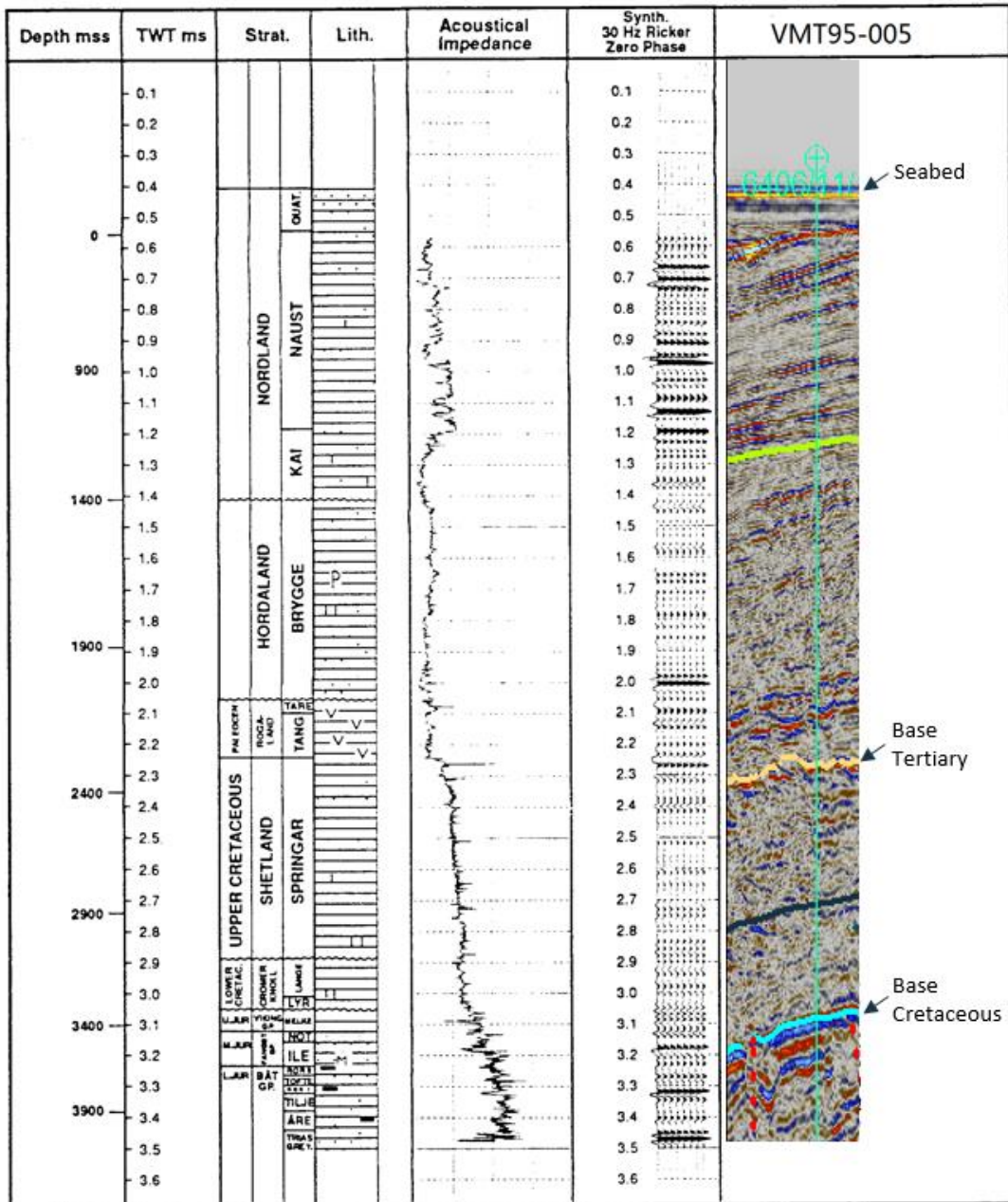
Figure 3.2: Well data of 6406/11-1S and example of picking selected horizons (modified from NPD[2])

4 Seismic Interpretation

In this chapter, we focus on the seismic interpretation of specific horizon related to the rifting process, including Base Cretaceous, Top Basement, Base Tertiary. Some notable reflectors, such as the intra-Cretaceous, sills, pre-Cretaceous reflector, intra-basement reflector 1, intra-basement reflector 2 and intra-basement reflector 3, and important faults will be interpreted as well. Table 1 gives an overview to the characters of these horizons in reflective seismic lines.
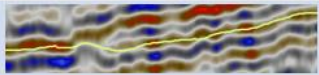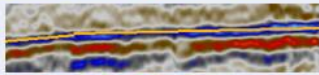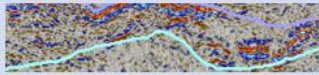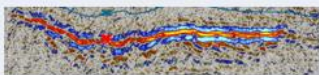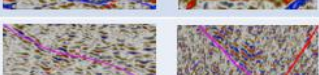
Horizons	Amplitude	Continuity	Examples
Intra-Tertiary	High	Good	
Base Tertiary	High	Good	
Lava Flow	High	Discontinuous	
Sills	High	Good	
Intra-Cretaceous	Variable	Good to moderate	
Base Cretaceous	High to moderate	Variable	
Pre-Cretaceous	High	Good	
Top Basement	Variable	Variable	
Intra-Basement Reflector 1	High to Moderate	Intermediate, locally discontinuous	
Intra-Basement Reflector 2	High to Moderate	Good to moderate	
Intra-Basement Reflector 3	High	Good	

Table 1: All interpreted horizons with typical characters and examples

The intra-Tertiary reflector is an important unconformity in the northern Møre Basin and Vøring Basin and shows a close relationship with Helland-Hansen Arch. The Base Tertiary is also the Top Cretaceous and important for estimating the thickness of Cretaceous sedimentary rocks. This horizon is picked based on the well data of 6306/6/1, 6404/11/1, 6406/8 and 6406/2/1 (shown in Figure 3.2). The lava flow is formed in the Early Tertiary and related with the final break-up. It can be found in most of the lines and shows a very high amplitude and chaotic facies. The intra-Cretaceous reflectors are identified by

26

comparing with the work of Zastrozhnov et al. (2020). The amplitude of four intra-Cretaceous reflectors are variable in different lines.

The Base Cretaceous shows a contact relationship of unconformity in the most deep basin area. Actually, the Base Cretaceous unconformity is the unconformity that separates the strata deposited in the extension phase of the Late Jurassic to the Early Cretaceous and later Cretaceous sediments, thus this unconformity should be actually the Early Cretaceous Unconformity. In this paper, we tentatively term it Base Cretaceous Unconformity with the abbreviation BCU. In the eastern of most line, the Base Cretaceous does not show the character of unconformity and is picked based on the well data.

In the Halten Terrace, the pre-Cretaceous reflector is pretty notable in the pre-Cretaceous sedimentary rocks. Most of the wells in Halten Terrace have drilled to Top Åre Fm., this reflector is below the Top Åre Fm., and we infer it as the Lower Jurassic reflector. In the deep basin area, this reflector is a rotated unconformity separating the syn-rift and pre-rift strata and is termed as pre-Cretaceous unconformity.

The Top Basement is a boundary of sedimentary rocks and igneous rocks. This reflector shows a high amplitude in the most parts of the lines. In some parts of the lines, the overlying sedimentary rocks might have experienced intense compaction, resulting in a weak contrast between the basement and overlying sedimentary rocks, thus the Top Basement is placed at the base of reflective sedimentary rocks in this situation. In the deep basin area, this reflector represents the top seismic basement due to lack of direct evidence to prove it as the top basement

The Middle Crust has a moderate contrast with the Upper Crust based on the work of Nirrengarten et al. (2014) in Møre Basin and is not continuous. Based on these two feature, we gave a possible inference that the intra-basement 1 reflector might be the Top Middle Crust in some lines. The intra-basement 2 is a reflector with high amplitude and good continuity and often cut by some large-scale normal faults. We will discuss the relationship between the Top Lower Crust and intra-basement 2. Moho is the boundary of the crust and mantle, this reflector often shows a high amplitude and is associated with hyperextension and, possibly, mantle exhumation caused by large-scale low-angle detachment faults in the study area. In some lines, we infer that the intra-basement 3 might be the Moho and will discuss it later.

4.1 VMT95-001

4.1.1 From Seabed to BCU
VMT95-001 is located in the south Møre Basin, paralleling to the northwestern parts of VMT95-002. With the comparison with VMT95-002, the Base Tertiary and four intra-Cretaceous reflectors are picked. The Base Tertiary reflector can be tracked to profile km c. 40 shown in Figure 4.1. The four intra-Cretaceous reflectors can be only tracked in the southeast parts of the line, probably caused by the variation of lithological characters or the impact of intrusive rocks.

4.1.2 BCU
Different to VMT95-002, an obvious onlap can be observed in the southeastern parts of the line near 6 s twt. The reflector with strong amplitude and good continuity onlapped by parallel sediment strata is recognized as unconformity and inferred as the Base Cretaceous Unconformity. This unconformity is interrupted by some faults inside the Ervik Ridge. In

the northwest of the Ervik Ridge, the Base Cretaceous can be tracked to profile km c. 60. In the northwest of F2, the poor quality of seismic profile caused by overlying lava flow makes the interpretation of Base Cretaceous impossible.

4.1.3 Top Basement

In the southeast parts of the line, a southeast-dipping reflector with a high amplitude is onlapped by the pre-Cretaceous sedimentary rocks, this reflector is recognized as the top seismic basement. In the northwest of the Ervik Ridge, the top seismic basement should be placed at a greater depth due to the impact of the normal fault F1. After comparing the VMT95-011, we tend to believe the depth of top seismic basement is larger than 10 s twt. In the northwest of F2, the poor quality of seismic profile caused by overlying lava flow makes the interpretation of deep reflectors impossible without other geophysical methods.

Below the top seismic basement, no reflectors with such a good continuity as the intra-basement 2 in VMT95-002 can be clearly observed. To the northwest of Ervik Ridge, a fault plane F2 is interpreted combining the SW-NE trending seismic line VMT95-011, which will be explained in Chapter 4.11.
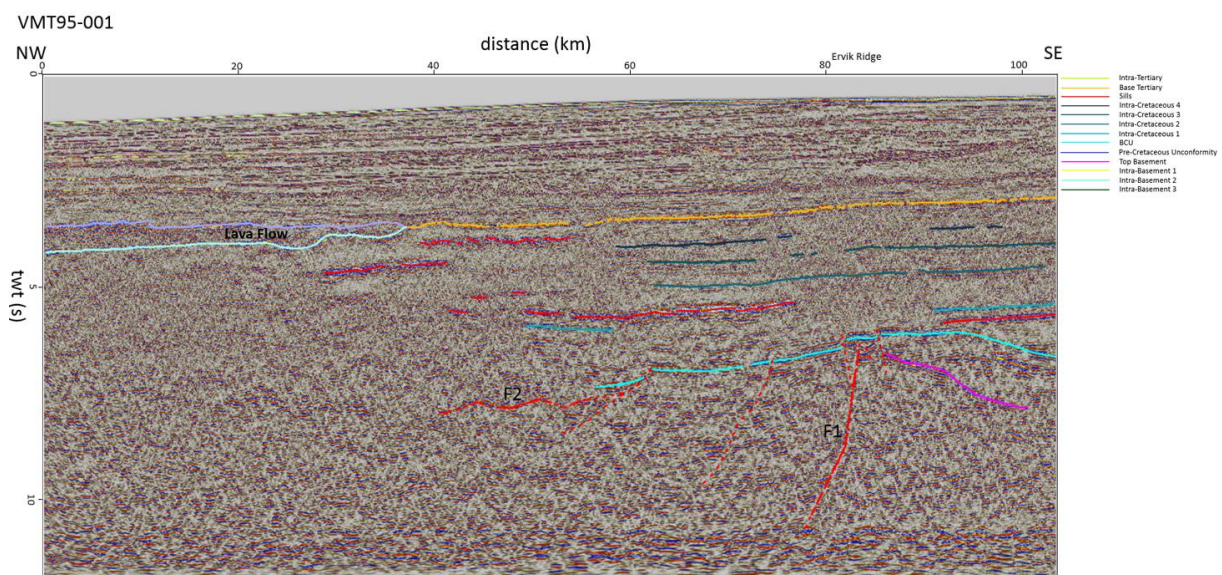
Figure 4.1: Seismic interpretation of VMT95-001

4.2 VMT95-002

4.2.1 From Seabed to BCU

Comparing with the line of VMT95-004, the Base Tertiary is picked, and with the target of deep structure, the sedimentary facies strata above the Base Tertiary will not be interpreted in details.

Due to the huge accommodation resulting from the large-scale normal fault, up to 4 s twt thickness of Cretaceous sedimentary rock can be observed in this seismic line. Four intra-Cretaceous reflectors with strong amplitude and good continuity have been interpreted, here tentatively terming intra-Cretaceous 1, intra-Cretaceous 2, intra-Cretaceous 3 and intra-Cretaceous 4 respectively. Zastrozhnov et al. (2020) detailedly interpreted the Cretaceous sedimentary rocks based on a great amount of regional correlation and long-offset 2D seismic reflection lines. By comparing with his work, the intra-Cretaceous 1-4

reflectors have been identified as base mid-Albian, intra mid-Cenomanian, intra lower-Coniacian and intra mid-Campanian respectively. In the northwestern parts, these Intra-Cretaceous reflectors become uncertain caused by intrusive rocks around 6 s twt.

4.2.2 BCU

In the southeastern parts of the line, between profile km c. 150 and 170, it is clear that an unconformity is onlapped by sedimentary rock at approximate 5s twt in Slørebotn Subbasin. This unconformity has a good continuity and moderate amplitude in the basin. The unconformity is interrupted by a well-imaged large normal fault in the southeast, which has a about 4 s twt vertical length producing an enormous sedimentary accommodation. In the Møre platform, this unconformity is cut by several high angle normal faults. With the combination of well data of 6306/6-1 in VMT95-004, this unconformity is interpreted as the Base Cretaceous Unconformity (Figure 4.2).

In the southeastern of Gnausen High, Base Cretaceous Unconformity is overlying above some normal faults which cut a northwest-dipping pre-Cretaceous unconformity. In the northwestern of Gnausen High, a 45 km acquisition gap occurs between the VMT95-002 and VMT95-002-, shown in Figure 4.2, making the tracking of Base Cretaceous difficult. From profile km c. 90 to 70 (Figure 4.2), a less clear onlap can be observed near 8 s twt. This unconformity is inferred as the Base Cretaceous Unconformity. The 1.5 s vertical displacement of BCU in the two sides of the acquisition gap may be caused by a moderate normal fault. Based on the displacement caused by normal fault near km c. 75, the Base Cretaceous is interpreted at a deeper reflector on the northwestern of the normal fault with a high uncertainty. Based on the gravity data, Osmundsen et al. (2016) found out that the strata between 6 to 10 s twt in the South Vigra High have a density of 2.75 , and proposed three kinds of scenarios about this strata These three scenarios are Continental crystalline crust, high-density Cretaceous sedimentary rocks and pre-Cretaceous strata respectively.

The South Vigra High is bounded by a large normal fault in the northwest which produced a huge sedimentary accommodation. Based on the possible displacement caused by the large normal fault, the Base Cretaceous is interpreted at the bottom of cretaceous sediments. This interpretation is also highly uncertain. In the northwestern parts, the overlying lava flow make the data quality in the underlying section quite low, the Base Cretaceous can't be recognized in this seismic line (Figure 4.2).

4.2.3 Top Basement

In the Møre Platform, the Top Basement is placed at a reflector near 2 s twt considering this area has only experienced a slight extension. From profile km c. 190, the Top Basement begins to drop dramatically due to the impact of a series high-angle normal faults. In the Slørebotn, a southeast-dipping reflector with high amplitude is incised by a large-scale normal fault F1. This reflector is located at the base of the pre-Cretaceous syn-rift sedimentary rocks and a weak onlap can be observed, thus it is recognized as the top seismic basement (Figure 4.2).

At profile km c. 140, a moderate amplitude reflector near 7 s twt separating the sediment and basement facies is interpreted as the top seismic basement. In the northwest of the acquisition gap, the top seismic basement is less well defined, and is placed at the bottom of reflective sedimentary rocks (Figure 4.2).

Figure 4.2: Seismic interpretation of VMT95-002

4.2.4 Intra-Basement Reflector

Below the top basement, two intra-basement reflectors are worth attention. In Møre Platform, an intra-basement reflector with moderated amplitude near 6.5 s twt can be observed. Nirrengarten et al. (2014) gave the seismic velocity, density and magnetic properties of the unites in Møre basin in his study (shown in Table 2). Based on the velocity and density in Table 1, the impedance difference between upper and middle crust can

Layer	Velocity (m/s)	Density (g/cm^3)	Susceptibility (SI)	Q
Water	1450	1.03	0	0
Cenozoic	1900–2300	2–2.35	0	0
Upper Cretaceous	2400–3500	2.25–2.4	0	0
Lower Cretaceous	3800–4700	2.4–2.6	0	0
Pre-Cretaceous	4900	2.6–2.65	0	0
Upper crust	6000–6300	2.75	0.001–0.015	0
Mid-crust	6500	2.83–2.88	0.02–0.05	0
Frøya remanent bodies	6500	2.85	0.03	0.7
Lower crust	7000	2.97	0.005	0
LCB	7200–7800	3.05–3.1	0.005	0
Sill		2.55	0.02	4
SDR	4500–5500	2.50–2.55	0.02	6
Upper oceanic crust		2.55	0.02	7
Lower oceanic crust		2.85	0.02	1
Mantle	>8000	3.275	0	0

Table 2: Seismic velocity, density and magnetic properties of different unites (Nirrengarten et al. 2014)

reach to 10% which is a moderate contrast. Based on this, we infer the intra-basement 1 reflector as the Top Middle Crust with a huge uncertainty resulting from lacking other geophysical data, such as gravity. From profile km c. 160 to 140, a southeast-dipping reflector with moderate to low amplitude can be observed and is inferred as the Top Middle Crust as well. The F1 could also develop along this reflector (Osmundsen et al., 2016).

Below the intra-basement 1, intra-basement 2 with a good continuity rises quickly from a depth of 10 s twt to the southeast end of the line to 8.5 s twt depth at profile km c. 180. This reflector can be tracked to the northwest end of the line. Near profile km c. 160 and 40, two large-scale normal faults seem to have incised into this reflector. It has a great possibility to be the Top Lower Crust (Figure 4.2).

4.3 VMT95-003

4.3.1 From Seabed to BCU
By the comparison with VMT95-002 and VMT95-004, the Base Tertiary and four intra-Cretaceous reflectors are picked and tracked throughout the seismic line. The continuity of intra-Cretaceous 4 is less good, it can be only partly identified probably resulting from the variation of lithological characters. In the west parts of the line, two reflectors with high amplitude are inferred as the sills, the lower one seems to coincide with intra-Cretaceous 3 reflector. In the Slørebotn Subbasin, the intra-Cretaceous 3 reflector is recognized, giving a possible inference that the Gossa High is formed earlier than geological time of intra-Cretaceous 3 which is the Early Coniacian according to the correlation work of Zastrozhnov et al. (2020).

4.3.2 BCU
The Base Cretaceous shows a geological contact relationship of unconformity in most parts of this seismic line and can be easily tracked. In the Slørebotn Subbasin, the Base Cretaceous Unconformity is the boundary of the Cretaceous sediments and pre-Cretaceous syn-rift sedimentary strata. From profile km 110 to 70, the Base Cretaceous shows a character of unconformity, possibly resulting from the uplifting and fault activities. In the western of the line, the activity of large-scale normal faults F1 and F2 leads to a greater depth of the Base Cretaceous. In the hanging wall of F2, a U-shaped reflector with moderate to high amplitude and moderate continuity is onlapped by the parallel facies Cretaceous sediments and is recognized as the BCU. In the South Vigra High, the Base Cretaceous shows a less clear character of unconformity, the Base Cretaceous is placed at the bottom of parallel facies Cretaceous sedimentary rocks (Figure 4.3).

4.3.3 Top Basement
In the Slørebotn Subbasin, two east-dipping reflectors with moderate amplitude can be observed in the hanging wall of the low-angle detachment fault. Considering the impact of detachment fault, the lower one is inferred as the Top Basement with some uncertainty. In the Gossa High, the Top Basement is placed the bottom of reflective sedimentary rocks. Following this interpretation, the Top Basement is place at the east-dipping or flat-lying reflector in the hanging wall of the west-dipping normal faults in the Ona High based on the displacement caused by these faults. In Ona High, the Top Basement reflector is cut by a series west-dipping low-angle faults. In the hanging wall F2, the Top Basement reflector is placed at the bottom of the pre-Cretaceous syn-rift sedimentary rocks and can be tracked to the westernmost parts of the line (Figure 4.3).
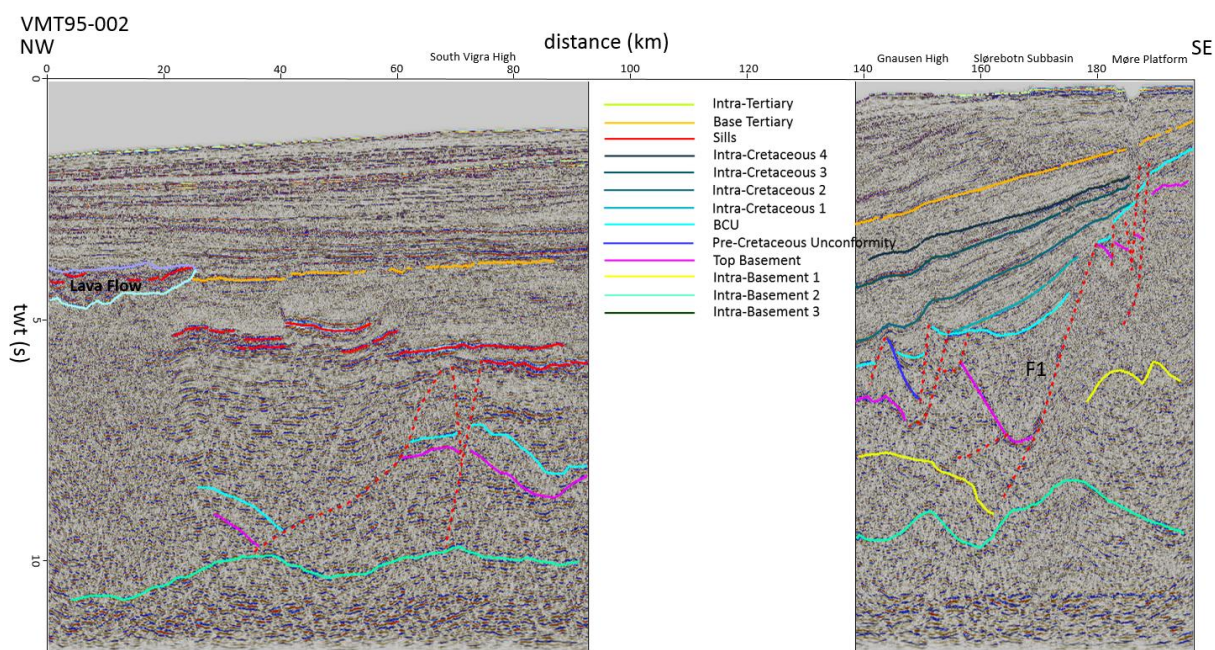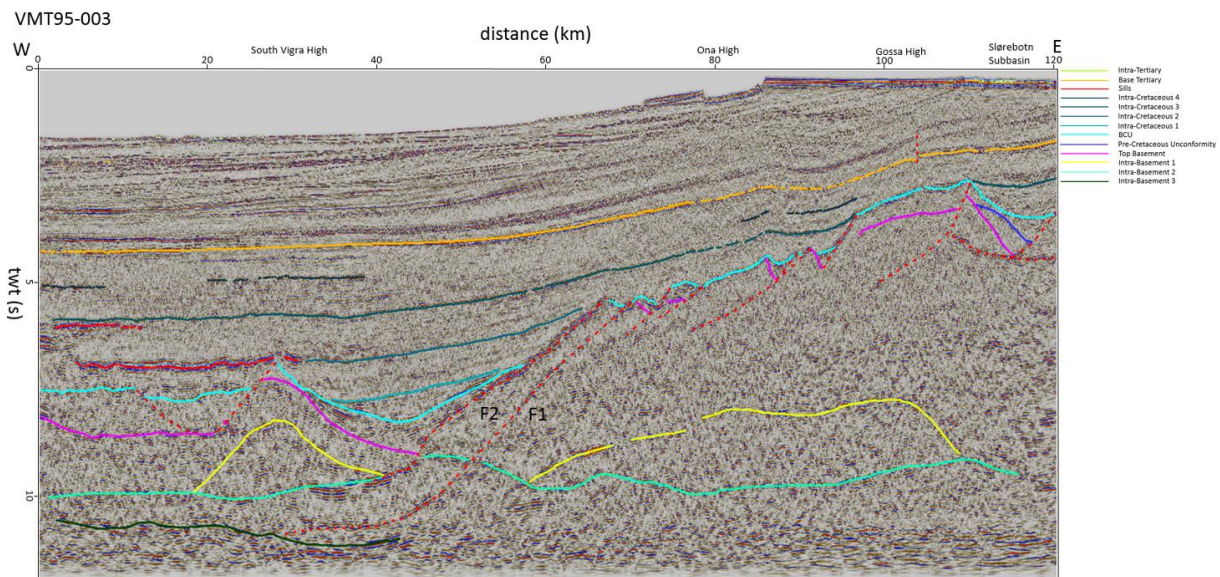
Figure 4.3: Seismic interpretation of VMT95-003

4.3.4 Intra-Basement Reflector

Below the Top Basement, some deep reflectors are also notable. From profile km c. 120-60, two reflectors near 9 s twt with good continuity and strong amplitude can be observed. The upper one intersects with the lower one at profile km c. 60 and 110. Considering the characteristic that the Middle Crust is not continuous, the two reflector is inferred as the Top Middle Crust and Top Lower Crust from upper to lower respectively. Between profile km c. 40 to 70, F1 incises into the Lower Crust and intersects with a deep reflector near 11 s twt. In South Vigra High, a triangle-shaped stratum can be observed below the Top Basement reflector, this stratum is interpreted as the Middle Crust by Nirrengarten et al. (2014) with the combination of gravity data. A flat-lying reflector with moderate continuity and amplitude is overlain by The Middle Crust and inferred as the Top Lower Crust. F2 also has a possibility to develop along this reflector. Below this reflector, another flat-lying reflector is located near 11 s twt and intersects with F1. This reflector is likely to be the Moho (Figure 4.3).

4.3.5 Slørebotn Detachment

Another notable structure is the detachment fault in the Slørebotn Subbasin. A flat-lying reflector with strong amplitude is recognized as low-angle detachment fault and named Slørebotn Detachment (Osmundsen & Ebbing, 2008). In the footwall of the detachment, a west-dipping secondary normal fault cuts into the wedge-shaped sedimentary strata. In the hanging wall of the normal fault, the upper east-dipping reflector is onlapped by slightly-dipping syn-rift sedimentary strata and recognized as the pre-Cretaceous unconformity (Figure 4.3).

4.4 VMT95-004

4.4.1 From Seabed to BCU

The exploration well 6306/6/1 is located in the east of the line and has been drilled to Jurassic strata. The Base Tertiary is picked according to the well data of 6306/6/1. The Base Tertiary can be easily tracked to profile km c. 40 due to the good continuity and high

amplitude. In the west parts of the line, the Base Tertiary becomes uncertain resulting from the existence of lava flow (Figure 4.4).

In the hanging wall of Klakk Fault Complex, four intra-Cretaceous reflectors are picked with the comparison with VMT95-002. From profile km c. 180 to 140, the less good data quality makes intra-Cretaceous reflectors unlikely to be identified. In the west parts of the line, the continuity of intra-Cretaceous 1 and 2 is good, but the intra-Cretaceous 3 and 4 can be only discontinuously identified. At profile km c. 100, a slightly-dipping reflector near 6 s twt with high amplitude is inferred as the sills. In the west parts of the line, similar reflectors can be observed and inferred as the sills as well (Figure 4.4).
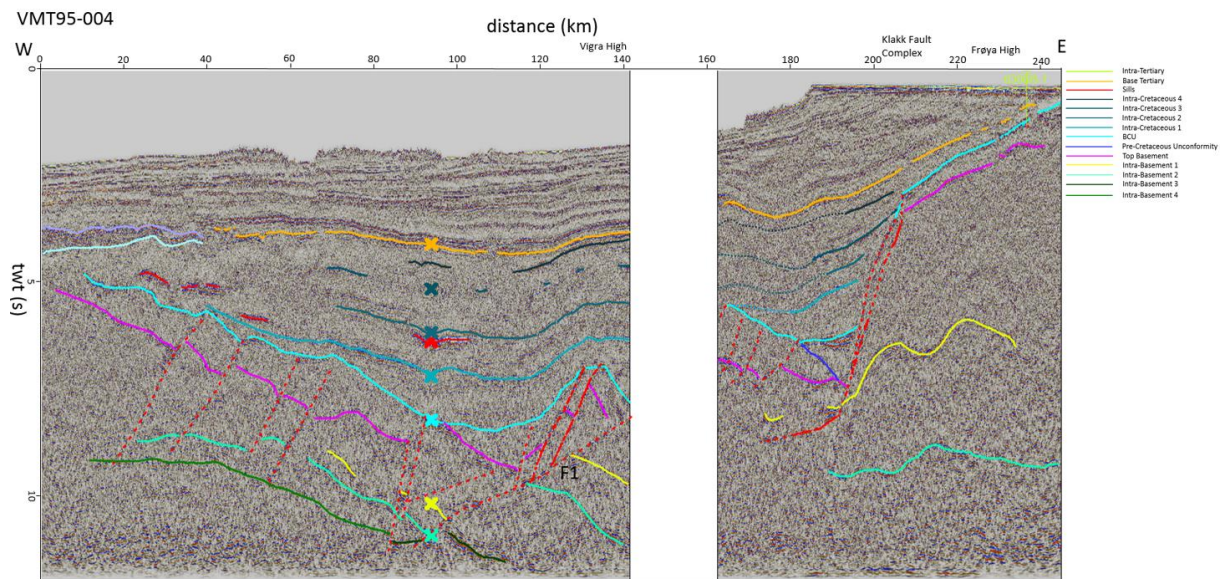
Figure 4.4: Seismic interpretation of VMT95-004

4.4.2 BCU
In the Frøya High, the Base Cretaceous reflector is identified with the well data of 636/6/1 and can be easily tracked until to the Klakk Fault Complex. The Klakk Fault Complex created a great accommodation for Cretaceous sediments. In hanging wall of Klakk Fault Complex, a flat-lying reflector with a strong amplitude and good continuity near 6 s twt begins to rise westwards and is onlapped by slightly west-dipping parallel facies sedimentary strata. This unconformity is inferred as the Base Cretaceous Unconformity. From profile km c. 160 to 140, a 20 km acquisition gap occurs between the VMT95-004 and VMT95-004-, making the tracking of Base Cretaceous more complex. In Vigra High, the east-dipping strata is overlain by parallel facies sedimentary rocks, and this obvious angular unconformity is identified as the Base Cretaceous Unconformity. In the west of Vigra High, this unconformity can be tracked to profile km c. 40. In the westernmost parts of the line, the Cretaceous sedimentary strata become ambiguous due to the overlying lava flow, the geological contact relationship between the Cretaceous and pre-Cretaceous strata can be hardly identified here (Figure 4.4).

4.4.3 Pre-Cretaceous Unconformity
In the hanging wall of Klakk Fault Complex, an east-dipping reflector is overlain by the wedge-shaped syn-rift pre-Cretaceous sedimentary rocks. This reflector is recognized as the pre-Cretaceous Unconformity and it intersects with the slightly-dipping Top Basement reflector (Figure 4.4).

4.4.4 Top Basement

In the Frøya High, a west-dipping reflector with strong amplitude and good continuity can be observed below the Base Cretaceous. This reflector is located at the base of parallel facies sedimentary strata in the footwall of the Klakk Fault Complex, thus inferred as the Top Basement. In the hanging wall of Klakk Fault Complex, the Top Basement intersects with the east-dipping pre-Cretaceous unconformity. From profile km c. 180-160, the Top Basement reflector is placed at the base of reflective sedimentary rocks and cut by a series west-dipping normal faults. In the Vigra High, a large-scale detachment fault F1 creates a series of secondary normal fault in its hanging wall. The top seismic basement is placed at the bottom of the east-dipping pre-Cretaceous sedimentary strata near profile km c. 140. Based on the displacement created by the secondary faults, the top seismic basement reflector is picked. From profile km c. 120 to 0, the top seismic basement is placed at the base of reflective sedimentary rocks due to the poor seismic data quality and it rises westwards, cutting by a series of west-dipping moderate normal faults (Figure 4.4).

4.4.5 Intra-Basement Reflector

Inside the basement, an undulated reflector with high amplitude near 7 s twt is inferred as the interior structure of basement and another possibility is the Top Middle Crust. Below this reflector, another undulated reflector is obvious near 9 s twt, it might be the Top Lower Crust. More geophysical method data can decrease the uncertainty of these two reflectors. Near 8 s twt, two high amplitude reflectors near profile km c. 180 is considered the same as the interior structure of basement in Frøya High.

In the footwall of F1, three east-dipping reflectors are notable. One possibility of these three reflectors is the Top Middle Crust, Top Lower Crust and Moho from top to bottom respectively. In the hanging wall of F1, these three reflectors are moved to a deeper place. The inferred Top Middle Crust reflector can be discontinuously observed to profile km c. 70. The amplitude of other two reflectors becomes moderate to weak from profile km c. 90. Considering the huge acoustic impedance between the mantle rock and lower crust, the lower reflector is unlikely to be the Moho. A possible inference is that it is the boundary of the Lower Crust and Altered mantle (Figure 4.4).

4.5 VMT95-005

4.5.1 From Seabed to BCU

The exploration well 6406/11/1 in Halten Terrace has penetrated the Cretaceous strata and reached to the Late Triassic strata. Using the data of exploration well 6406/11/1, the Base Tertiary is picked and an unconformity inside Tertiary can be observed, tentatively terming intra-Tertiary Unconformity.

Comparing the VMT95-004, the four intra-Cretaceous reflectors are picked in the most parts of the line. From profile km c. 170 to 120, the poor-imaged Cretaceous strata make the tracking of intra-Cretaceous 3 and 4 complex. Near profile km c. 60, the amplitude of intra-Cretaceous 1 becomes obviously higher, inferred as the impact of intrusion rocks. In the westernmost of the line, a reflector with strong amplitude and moderated continuity rises westwards and interpreted as the sills, the intra-Cretaceous 1 reflector is probably near this reflector even coincides with this reflector (Figure 4.5).

In Frøya High, the thickness of Cretaceous sediments is only 0.5 s twt. However, a series of normal fault including F1, F2 and F3 creates huge accommodation for Cretaceous

sediments. In the west of Grip High, the thickness of Cretaceous sediment can reach to 4.5 s twt. Near the Grip High, two anticlines can be observed, possibly resulting from the compression in Tertiary but before the time of intra-Tertiary Unconformity. Another thing that needs to be noticed is that no lava flow appears in the west of the line (Figure 4.5).

4.5.2 BCU

With the well data of 6406/1/1, the Base Cretaceous is easily identified with no uncertainty in Halten Terrace. And in this line, it has a high amplitude and good continuity. Near profile km c. 210, the F1 bounding the Halten Terrace in the east is interpreted as a detachment fault resulting in a 0.7 s twt displacement of the Base Cretaceous. In Frøya High, the Base Cretaceous reflector has a better continuity and higher amplitude than Halten Terrace. In the west boundary of Halten Terrace, Klakk Fault Complex (noted as F2 in Figure 4.5) produced a considerable deposition accommodation for Cretaceous strata. In the hanging wall of F2, an unconformity onlapped by sedimentary rocks near 6 s twt is interpreted as the Base Cretaceous Unconformity. At profile km c. 160, another normal fault makes the thickness of Cretaceous sediments greater. An unconformity onlapped by sedimentary rocks near 7 s twt is recognized as Base Cretaceous Unconformity (Figure 4.5).

In the Grip High, A 10 km acquisition gap interrupted the seismic line. In the hanging wall of a west-dipping fault, an east-dipping unconformity is interpreted as the Base Cretaceous Unconformity. This reflector is cut by another west-dipping normal fault then rise westwards to the footwall of F3. In the hanging wall of F3, the resolution is not that good as the eastern parts of the seismic line. The Base Cretaceous Unconformity is interpreted at the bottom of the parallel facies strata near 7 s twt. In the westernmost of the line, the Base Cretaceous is placed at an east-dipping reflector near 6 s twt but not reliable anymore due to the impact of overlying intrusion rocks (Figure 4.5).
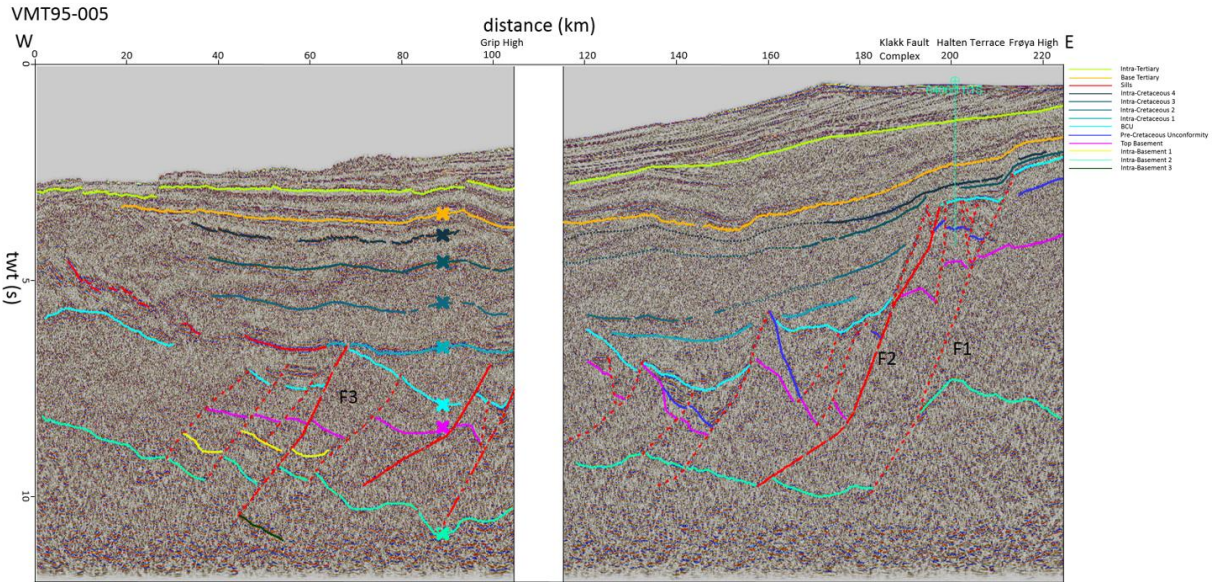
Figure 4.5: Seismic interpretation of VMT95-005

4.5.3 Pre-Cretaceous Unconformity

In this line, we identified some notable pre-Cretaceous reflectors. In the Halten Terrace, the well 6406/1/1 has drilled to the Late Triassic strata. Near the well, a flat-lying reflector with a good continuity and high amplitude is named pre-Cretaceous reflector. This reflector can be well tracked in the Halten Terrace and in the footwall of F1 (Figure 4.5).

35

From profile km c. 180 to 140, two wedge-shaped reflector packages, interpreted as syn-rift sedimentary strata, are notable. At the base of these two sedimentary strata, two east-dipping reflectors are recognized as the unconformity, termed pre-Cretaceous unconformity here (Figure 4.5).

4.5.4 Top Basement

In Halten Terrace, considering that the exploration well has penetrated into the Triassic strata., the Top Basement is placed at the bottom of reflective sedimentary rocks near 4.5 s twt below the bottom of the well. In the east of the well, the large normal fault F1 defining the east of Halten Terrace is thought to have cut into the basement, giving the evidence for interpreting the reflector near 4.2 s twt in the footwall of F1 as the Top Basement. In the west parts of Halten Terrace, the Top Basement goes deeper along moderate faults in the west of the well (Figure 4.5).

At profile km c. 180, the top seismic basement is placed at a rotated reflector in the hanging wall of large-scale normal fault. This large-scale normal fault is Klakk Fault Complex here, it produces two west-dipping secondary normal faults incising into the top seismic basement reflector. In the small subbasin near profile km c. 140, the top seismic basement is interpreted at the bottom of the pre-Cretaceous sediments and inferred to rise westwards in Grip High then go deeper due to the impact of the large normal fault bounding the west of Grip High (Figure 4.5).

In the west of Grip High, the data quality becomes less good. The top seismic basement shows a high to moderate amplitude and intermediate to discontinuous continuity and is tentatively placed at the base of reflective sedimentary rocks. From profile km c. 40 to 0, the Top Basement cannot be recognized anymore (Figure 4.5).

4.5.5 Intra-Basement Reflector

Below the Top Basement in Frøya High, an intra-basement reflector with a high amplitude near 7.5 s twt is inferred as the Top Lower Crust with a great uncertainty. In the hanging wall of F1, near 10 s twt, a gently dipping reflector can be observed. Considering the possibility that F1 incises is likely to incise into Lower Crust, this reflector is inferred as the Top Lower Crust. In the hanging wall of Klakk Fault Complex, this reflector can be tracked to profile km c. 120 (Figure 4.5).

In the west of the acquisition gap, an undulated reflector with high amplitude and intermediate continuity is cut by a large-scale normal fault near profile km c. 100. This reflector is inferred as the Top Lower Crust. Considering a 1 s displacement of the Top Lower Crust in the two sides of the acquisition gap, it is likely that a normal fault exists in the acquisition gap. From profile km c. 80 to 40, the Top Lower Crust is cut by a series west-dipping normal faults, including F3. In the westernmost of the line, the Top Lower Crust has a trend to rise westwards, but the poor-imaged seismic makes the exact location of Top Lower Crust pretty uncertain (Figure 4.5).

From profile km c. 80 to 40, some flat-lying reflectors between the Top Basement and Top Lower Crust with high to moderate amplitude can be observed, we give it a possible inference of the Top Middle Crust. In the footwall of F3, intra-basement 3 can be observed near 10.5 s twt, and F3 seems to have touched this reflector. In the footwall of F3, this reflector cannot be observed anymore. Based on the observation, we give a probable inference that this reflector is likely to be the boundary of Lower Crust and Altered mantle

and F3 has incised into altered mantle, due to the boundary effect in the data processing, this reflector is covered by the boundary reflection noise (Figure 4.5).

4.6 VMT95-006

4.6.1 From Seabed to BCU
In Halten Terrace, well 6406/8/1 has drilled to the Lower Jurassic strata near 5 s twt. In the east of the seismic line, a reflector with high amplitude and good continuity is overlain by clinoform facies sediments, recognized as the Top Tertiary from the well data of 6406/8/1. Following this feature, the Top Tertiary reflector is picked throughout the line. Near profile km c. 100, an anticline is overlain by this reflector, this anticline also shows in VMT95-007 and VMT95-008.

At 2.7 s twt, the Base Tertiary is picked according to the well data of 6406/8/1 as well. From profile km c. 150 to 110, the Base Tertiary reflector cannot be accurately tracked due to the poor seismic quality in this area.

In the hanging wall of Klakk Fault, four intra-Cretaceous reflectors have a moderate to high amplitude and moderate continuity. In the most parts of seismic line, the intra-Cretaceous 4 reflector has a better continuity and higher amplitude than other three reflectors. From profile km c. 80, the intra-Cretaceous 2 and 3 becomes ambiguous caused by the sills.

From profile km c. 40 to 0, a notable undulated reflector with a high amplitude near 3.5 s twt is inferred as lava flow with an uneven surface overlain by the Tertiary sedimentary rocks. Below the lava flow, some seaward to gently dipping reflectors is conspicuous. Two possible interpretations about this reflector are provided. First, this reflector represents inner structure of basalt flow. Second, it is the sill intruding in poorly imaged sedimentary rocks (Figure 4.6a).

4.6.2 BCU
In Halten Terrace, a reflector with a high amplitude and good continuity onlapped parallel facies sedimentary rocks is interpreted as the Base Cretaceous, confirmed by well data of 6406/8/1. In the hanging wall of Klakk Fault Complex, near profile km c. 160, a flat-lying reflector with moderate amplitude separates the parallel facies sedimentary rock and underlying west-dipping syn-rift sedimentary strata, this reflector is recognized as angular unconformity and interpreted as the Base Cretaceous Unconformity. From profile km c. 160 to 120, two east-dipping reflectors are onlapped by the Cretaceous sedimentary strata. These reflectors are separated by a moderate normal fault and inferred as the Base Cretaceous Unconformity. The western boundary of Grip High is a moderate fault resulting in a larger depth of the Base Cretaceous. From profile km c. 120 to 60, a reflector with low to moderate amplitude near 7 s twt is onlapped by parallel facies sedimentary strata and inferred as the Base Cretaceous Unconformity. Near profile km c. 50, an east-dipping reflector is interpreted as a normal fault. In the footwall of this fault, the Base Cretaceous becomes ambiguous caused by the overlying igneous rocks (Figure 4.6a).

4.6.3 Pre-Cretaceous Unconformity
In the Halten Terrace, two pre-Cretaceous reflectors with strong amplitude are picked based on the well data of 6406/8/1. In the west, these two reflectors are cut by a normal fault. In the hanging wall of this fault, the quality of seismic data becomes less good, no obvious pre-Cretaceous reflectors can be picked. In the west of the Klakk Fault Complex,

we provide a possibility about the pre-Cretaceous unconformity (shown in Figure 4.6b) in the next subchapter.

4.6.4 Top Basement and Intra-Basement Reflector

In the Halten Terrace, well 6406/8/1 has drilled to the Lower Jurassic strata near 5 s twt. Based on this, the Top Basement is placed at a east-dipping reflector located at the base of reflective pre-Cretaceous sedimentary rocks. In the footwall of Klakk Fault Complex, it is cut by a normal fault and drops westwards.

In the west of Klakk Fault Complex, two scenarios about the deep reflectors below the Base Cretaceous have been proposed (shown in Figure 4.6 a and b).
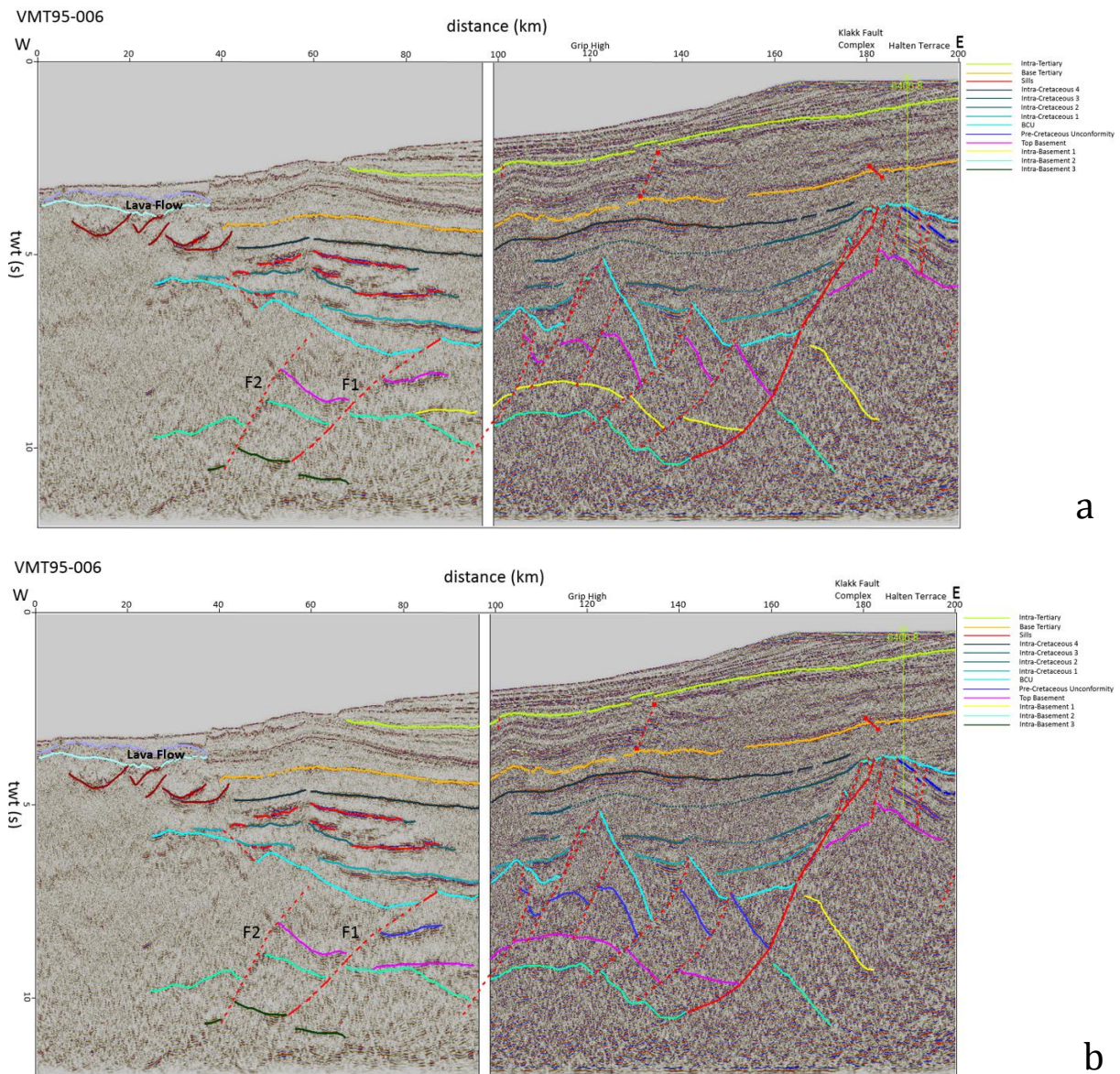

Figure 4.6: Seismic interpretation of VMT95-006

The first one is shown in Figure 4.6a. The Klakk Fault Complex cuts into an east-dipping reflector overlain by a wedge-shaped succession of pre-Cretaceous sediments. This reflector is tentatively interpreted as the top seismic basement in this scenario and defined

by a moderate normal fault in the west. In the hanging wall of this fault, the top seismic basement is placed at the base of reflective sedimentary rocks. In the Grip High, a well-imaged small normal fault, which is inferred to be active in the early stretching phase before the activation time of Klakk Fault Complex, separates an east-dipping reflector and a flat-lying reflector. These two reflectors are overlain by pre-Cretaceous sedimentary rocks and inferred as the top seismic basement. Below the top seismic basement, two reflector is notable. The upper one has a poor continuity and moderate amplitude. The lower one has a high amplitude and poor to moderate continuity. Both two reflectors can be tracked from profile km c. 160 to 80. These two reflectors are inferred as the Top Middle Crust and the Top Lower Crust respectively in this scenario. Near profile km c. 80, the Top Middle Crust converges with the Top Lower Crust, coinciding with the Middle Crust' s character of discontinuity.

The second one is shown in Figure 4.6b. The differences between these two scenarios are the interpretation of the pre-Cretaceous unconformity, Top Basement and Top Middle Crust. From profile km c. 160 to 120, near 7 s twt, three east-dipping reflectors are picked. These reflectors are overlain by reflective sedimentary rocks. Below these reflectors, it is difficult to recognize the seismic facies of the strata. After a rough estimation, the thickness of pre-Cretaceous sedimentary rocks in Halten Terrace is about 2 s twt. The thickness of sedimentary rocks in the hanging wall of Klakk Fault should be greater than 2 s twt under the condition that the Klakk Fault Complex has created a substantial deposition accommodation for pre-Cretaceous syn-rift sediments. Based on this reason, the three east-dipping reflectors are interpreted as pre-Cretaceous unconformity and the reflector with a high amplitude and moderate continuity below the pre-Cretaceous unconformity is interpreted as the Top Basement in this scenario. Below the pre-Cretaceous unconformity, the pre-Cretaceous strata don' t show any typical characters of sedimentary facies in the seismic image, possibly resulting from the intense compaction and high-frequency fault activities.

In the hanging wall of F1, the top seismic basement is placed at the reflector at 8 s twt with great uncertainty. In the west of F2, the Top Basement cannot be tracked anymore.

From profile km c. 190 to 170, two deep reflectors rise westwards dramatically and are inferred as the Top Middle Crust and Top Lower Crust respectively. In the hanging wall of Klakk Fault Complex, the Top Middle Crust is of high uncertainty from profile km c. 160 to 80 and some inferrence is given above (shown in Figure 4.6a). The Top Lower Crust can be tracked to profile km c. 70 and a possibility about it is that from profile km c. 150 to 120, the Klakk Fault Complex may develop along the Top Lower Crust reflector.

In the hanging wall of F1, the Top Lower Crust is placed at a deeper slightly dipping reflector with moderate to high amplitude. In the west of F2, a west-dipping reflector is inferred as the Top Lower Crust with great uncertainty. Below the Top Lower Crust, a gently dipping reflector with moderate to high amplitude are separated by F1 and F2 and inferred as the Top Altered Mantle, giving a possible evidence of mantle exhumation in this seismic line.

4.7 VMT95-007

4.7.1 From Seabed to BCU
With the well data of 6406/2/1, the Base Tertiary and intra-Tertiary reflector are picked. And the intra-Tertiary reflector is confirmed as the Base Pliocene. In the east parts of the

line, the intra-Tertiary is downlapped by parallel to divergent facies sediment strata. Near profile km c. 120, an anticline is notable, and the intra-Tertiary is placed at the top of the anticline. In the west parts of the line, it can be tracked to profile km c. 30. Notably, at profile km c. 60, the intra-Tertiary reflector is onlapped by parallel facies sedimentary rocks, this unconformity is probably related with the underlying lava flow formed in the Early Tertiary (Figure 4.7).

The Cretaceous sedimentary rocks in this seismic lines is obviously thicker than other seismic lines even in the Halten Terrace. Same as other profiles, 4 intra-Cretaceous reflectors are picked by comparing with the other seismic lines. Obviously, the thickness between the intra-Cretaceous 4 and Base Tertiary is particularly greater than other profiles. A reflector with good continuity and strong amplitude is picked and termed as intra-Cretaceous 5 (Figure 4.7).

4.7.2 BCU

In the Halten Terrace, an unconformity near 4 s twt in the Halten Terrace is interpreted as the Base Cretaceous Unconformity, confirmed by well data of 6406/2/1. This Base Cretaceous Unconformity is interrupted by a series of small normal faults form in the early stretching phase.

In the hanging wall of Klakk Fault, near 7 s twt, a reflector with high amplitude and low to moderate continuity is onlapped by parallel facies sedimentary strata and can be tracked to the Slettringen Ridge. This reflector is interpreted as the Base Cretaceous Unconformity and rises westwards to Slettringen Ridge (Figure 4.7).

The western boundary of Slettringen Ridge is a normal fault. Due to the acquisition gap, this normal fault can't be fully sketched. However, this fault indeed creates a huge deposition accommodation for Cretaceous sediments and is important for recognizing the Base Cretaceous. In the hanging wall of F2, a slight-dipping reflector with high to moderate amplitude is cut by two secondary faults of F2. This reflector is located the base of the Cretaceous sedimentary rocks and is the boundary of Cretaceous strata and pre-Cretaceous strata. After considering F2 is active before the geological time of the Base Cretaceous Unconformity, based on that F2 is covered by Base Cretaceous in its footwall, we infer that the slight-dipping reflector is the Base Cretaceous Unconformity (Figure 4.7).

In the footwall of F3, the seismic image becomes ambiguous. The Base Cretaceous is placed at a reflector near 6 s twt with a great uncertainty. From profile km c. 60, very little information in large depth can be obtained from seismic reflective profile (Figure 4.7).

4.7.3 Pre-Cretaceous Unconformity

In Halten Terrace, the exploration well 6406/2/1 has drilled to the Early Jurassic strata. Near the well, the east-dipping parallel pre-Cretaceous sedimentary strata are incised by a normal fault F1. In the east of F1, we name a reflector with high amplitude and good continuity as pre-Cretaceous reflector. This reflector is cut by some small normal faults formed in the early stretching phase. In Sklinna Ridge, the pre-Cretaceous reflector is placed at a high-amplitude reflector near 5 s twt. In the hanging wall of Klakk Fault, this reflector drops to 8 s twt, incised by a secondary normal fault of Klakk Fault Complex. In the hanging wall of this fault, an east-dipping reflector is onlapped by wedge-shaped syn-rift sedimentary strata and inferred as the pre-Cretaceous Unconformity (Figure 4.7).

4.7.4 Top Basement

In the footwall of F1, the Top Basement is placed at the base of this pre-Cretaceous strata. In the hanging wall of F1, great amounts of small faults have been interpreted based on the different dipping angle of pre-Cretaceous sedimentary rocks, making the signal less good below these fault. Following the place of Top Basement in the footwall of F1, the reflector located at the end of F1 is inferred as the Top Basement with some uncertainty, this reflector is also likely to be the possible extension of F1 (Figure 4.7).
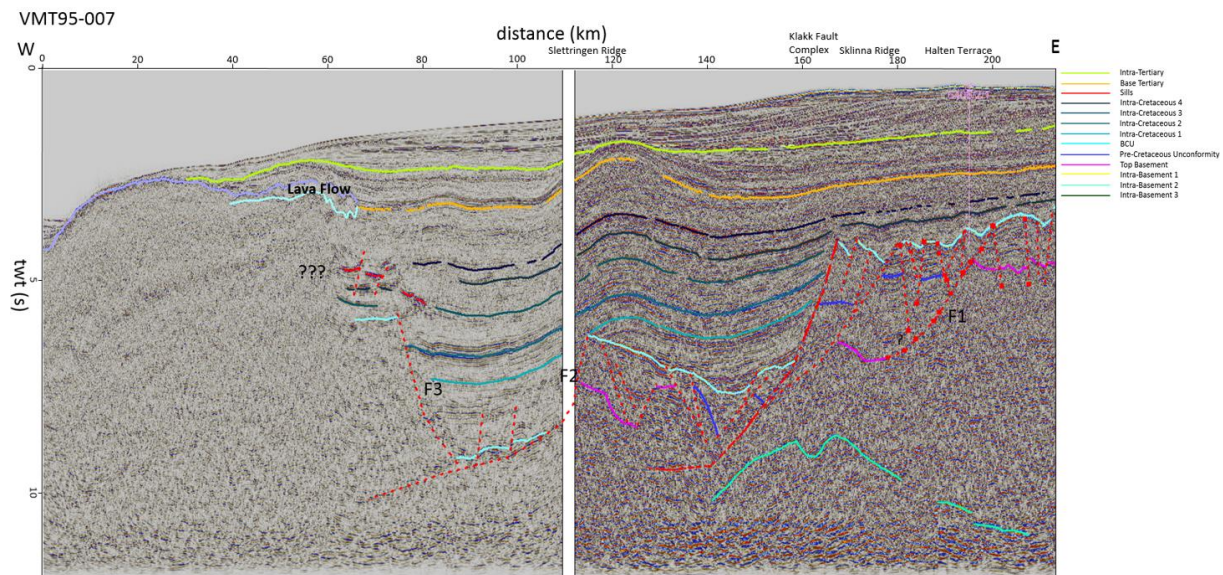
Figure 4.7: Seismic interpretation of VMT95-007

Form profile km c. 160 to 140, we cannot find the possible Top Basement reflector. Near profile km c. 130, a boundary separating the sedimentary rocks and chaotic facies strata is defined by two faults in the west and east respectively. This boundary is inferred as the top seismic basement. In Slettringen Ridge, the top seismic basement rises westwards, then descends to a great depth with the impact of F2. In the west of the acquisition gap, the Top Basement cannot be recognized anymore (Figure 4.7).

4.7.5 Intra-Basement Reflector

In the easternmost of the profile, near 11 s twt, a reflector with a strong amplitude rises westwards to 9 s twt from km c. 210 to 170 and is inferred as the Top Lower Crust. Near profile km c. 170, this reflector goes deep with a probable influence of Klakk Fault Complex. In the west of Klakk Fault Complex, this reflector cannot be tracked. In this line, a very strong amplitude reflector near 11s twt can be tracked throughout the line, it is inferred as the boundary noise based on its flat shape (Figure 4.7).

4.7.6 Helland-Hansen Arch

Near profile km c.120, an anticline is overlain by the intra-Tertiary reflector. This anticline has a good extension in 3D space and can be observed in VMT95-006 and VMT95-008. The center of this anticline may be close to VMT95-007, based on the different curvature in three seismic lines. Considering the anticline is covered by the intra-Tertiary reflector, which is exactly the Base Pliocene, it is inferred that a compression in the Early Tertiary but before Pliocene may contribute to it. This anticline is called Helland-Hansen Arch (Figure 4.7).

4.8 VMT95-008

4.8.1 From Seabed to BCU

In the easternmost of the line, an anticline is overlain by a reflector with good continuity and high amplitude onlapped by parallel sedimentary strata. This anticline is recognized as the Helland Hansen Arch in the structure element map. In the line VMT95-007, the Helland Hansen Arch is overlain by the Pliocene sedimentary strata with the calibration of well data 6406/2/1. Thus, in VMT95-008, the reflector lying above the Helland Hansen Arch is termed as the intra-Tertiary reflector. In the west of the line, this reflector becomes flat-lying and parallel to the overlain sedimentary strata. Below the intra-Tertiary reflector, the Base Tertiary reflector is picked with some uncertainty through comparing the Base Tertiary reflector in VMT95-007. Near profile km c. 25, the Base Tertiary reflector is overlain by the lava flow, indicating the lava flow is formed in the Early Tertiary (Figure 4.8).

In the hanging wall of Fles Fault Complex, three intra-Cretaceous reflectors are recognized by comparing with the VMT95-007. Between the intra-Cretaceous 3 and Base Tertiary, the thickness of Cretaceous sedimentary strata can reach to 2 s twt, but due to lack of well data it is difficult for a further classification. In the west of the Vigrid Syncline, the three intra-Cretaceous reflectors have a convergent trend which is not very clear due to the impact of the normal fault near profile km c. 30 (Figure 4.8).
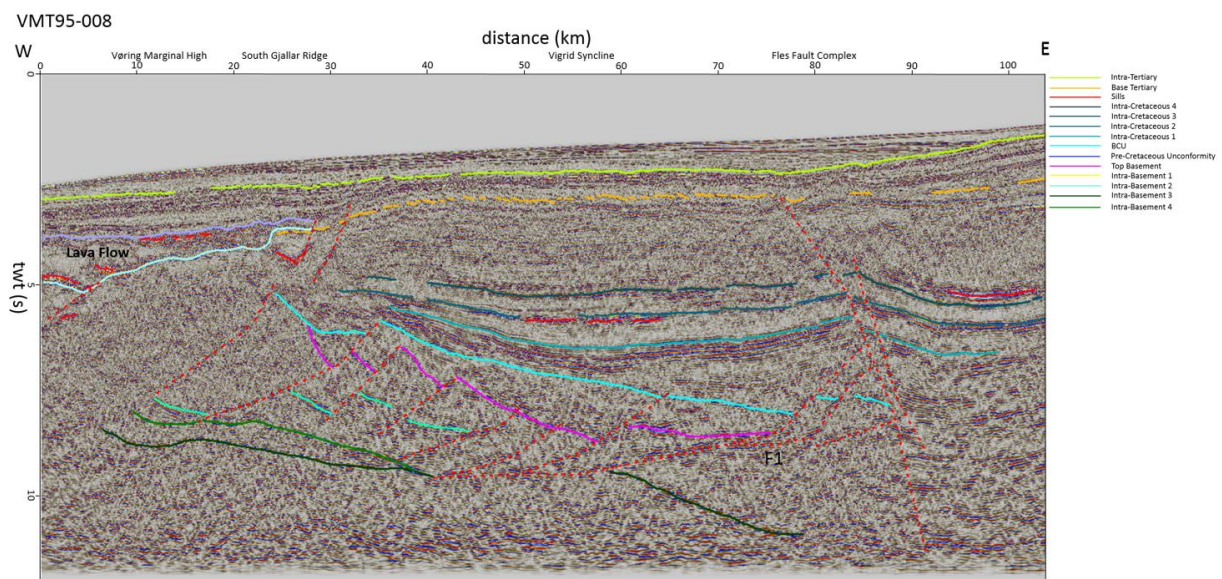
Figure 4.8: Seismic interpretation of VMT95-008

4.8.2 BCU

In the westernmost of the line, the Base Cretaceus cannot be recoginzed due to the impact of the lava flow. From profile km c. 25-75, an east-dipping reflector with moderate to low amplitude and less good continuity near 7 s twt can be observed and onlapped by the Cretaceous sedimentary strata. This reflector is interpreted as the Base Cretaceous Unconformity. Near profile km c. 80, this reflector is cut by a secondary normal fault of F1, and the Base Cretaceous reflector is placed at a slight-dipping reflector with modeate amplitude, with the consideration that F1 and its secondary fault have created a small displacement to the Base Cretaceous reflector. In the hanging wall of Fles Fault Complex, the sedimentary facies strata can reach down to 11 s twt resulting from the activity of the

Fles Fault Complex. Little direct evidence about the Base Cretaceous can be found here (Figure 4.8).

4.8.3 Top Basement and Intra-Basement Reflector

In this line, the top seismic basement can be only recognized between profile km c. 30 to 80. In this area, the top seismic basement is placed at the base of pre-Cretaceous sedimentary strata and cut by a series west-dipping normal faults. From profile km c. 15 to 45, some east-dipping reflectors with strong amplitude and good continuity near 8 s twt are cut by this series west-dipping normal faults as well and inferred as the Top Lower Crust (Figure 4.8).

Notably, near 9 s twt, a slightly dipping reflector can be observed from profile km c. 40 to 80, this reflector seems to have influenced the overlain strata and structures to a greater or less degree. In this thesis, it is identified as the low-angle detachment fault based on reflective seismic data. Based on the seismic reflective and gravity data, Osmundsen et al. (2016) proposed that this reflector is the boundary of strata with density of 2.85   and 3.1. As to these two different density strata, he proposed three kinds of possibilities. The first one is that the upper strata is continental crystalline crust and the lower one is high-density continental crust. The second one is that the upper strata is continental crystalline crust and the lower one is altered or intruded mantle rocks. The third one is that the two strata are altered or intruded mantle rocks with different density. Zastrozhnov et al. (2020) proposed an interpretation that detachment faults in the Rån Ridge and Hevring High could develop along the Permian-Triassic evaporites.

From profile km c. 80, a reflector with moderate amplitude rises westwards to the footwall of F1. Without the constrain of other geophysical data, two possibilities with great uncertainty are given here. The first one is the top altered mantle, based on the strong crust thinning caused by the low-angle detachment fault. The second one is the Top Lower Crust.

From profile km c. 40 to 10, below the Top Lower Crust, two slightly dipping reflectors are picked. As to these two reflectors, Osmundsen et al. (2016) proposed that the upper one is the boundary of altered mantle and overlain strata and the lower one is the interior altered mantle structure. Without the constrain of other geophysical data, two possibilities with great uncertainty are given here. The first one is that the upper one is the top altered mantle and the lower one is Moho, considering the mantle exhumation after intense crust thinning caused by large-scale low-angle fault F1. The second possibility is that the upper reflector is the extension of low-angle detachment fault and the lower reflector is the top altered mantle.

4.9 VMT95-009

The VMT95-009 is N-S trend line and located to the northeast of VMT95-008. Comparing with VMT95-008, three intra-Cretaceous reflectors and Base Tetiary are picked in the south parts of the line then tracked throughout the line. In the north parts of the line, the Fles Fault Complex creates about 1 s twt displacement to the three intra-Cretaceous reflectors and the thickness of the sedimentary rocks can reach to 9 s twt.

Near profile km c. 30, an onlap can be observed at 10 s twt. Based on this feature, the Base Cretaceous is placed at the bottom of the parallel sedimentary strata. In the footwall of Fles Fault Complex, the Base Cretaceous is picked according the displacement created by the Fles Fault Complex. However the activity of Fles Fault Complex may vary in different

period, this interpretation is likely of great uncertainty. Near profile km c. 70, a north-dipping reflector with moderate amplitude and good continuity near 10 s twt is onlapped by parallel sedimentary strata and interpreted as the Base Cretaceous Unconformity. It can be tracked in the footwall of a south-dipping normal fault located in the northernmost of the line as well (Figure 4.9).

In the hanging wall of Fles Fault Complex, a reflector with weak moderate amplitude and good continuity below the Base Cretaceous separates the pre-Cretacous strata and chaotic facies strata, and is inferred as the top seismic basement. This reflector can be tracked in the hanging wall of Fles Fault Complex (Figure 4.9).
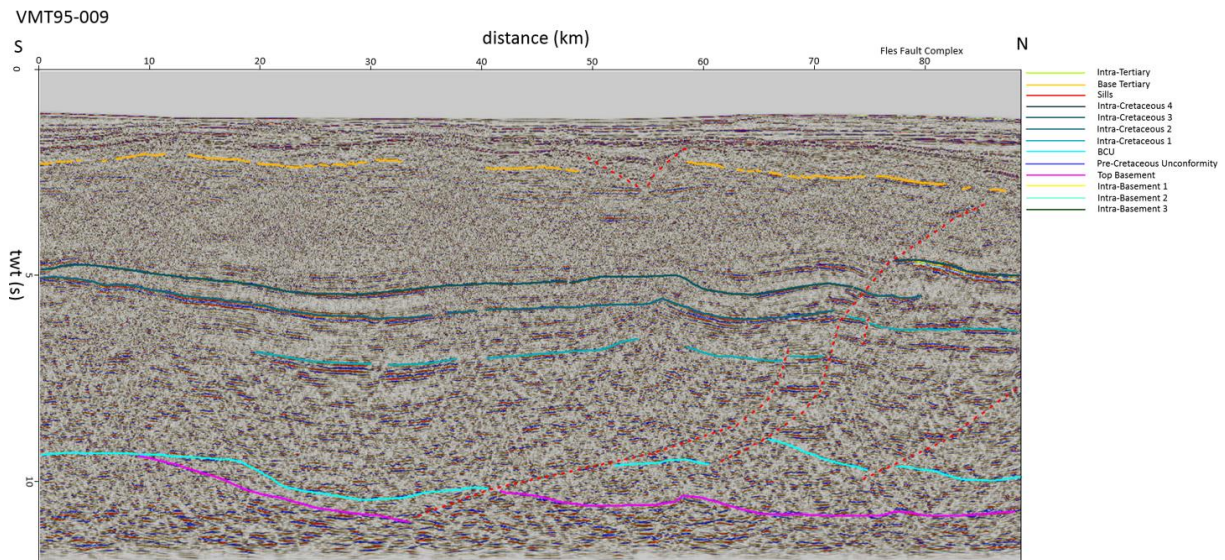
Figure 4.9: Seismic interpretation of VMT95-009

4.10 VMT95-010

The VMT95-010 is a NE-SW trend line and located in the northwest of Vigra High, penetrating the western parts of VMT95-004 and VMT95-005. This line is perpendicular to the direction of rifting propagation, providing a sight to the extension of important horizons and faults in 3D space.

4.10.1   From Seabed to BCU

Comparing with VMT95-005 and VMT95-004, the Base Tertiary and 4 intra-Cretaceous reflectors are picked and tracked throughout the line. In the southwest parts of the line, the intra-Cretaceous 4 reflector is not able to be recognized due to the variation of lithological characters. Near profile km c. 45, a high amplitude reflector with a length of near 20 km is identified as the sills. In the southwest parts of the line, a high amplitude reflector with 10 km length is inferred as the sills as well (Figure 4.10).

4.10.2   BCU

Comparing with the interpretation of VMT95-005, the Base Cretaceous reflector is picked. Different with VMT95-005, the Base Cretaceous does not show a contact relationship of unconformity at the intersection point. From profile km c. 70 to 10, the Base Cretaceous is onlapped by the parallel sedimentary strata recognized as the Base Cretaceous Unconformity and can be easily tracked in this area. In the intersection point with VMT95-

004, the location of the Base Cretaceous reflector can accurately match the interpretation of VMT95-004 (Figure 4.10).
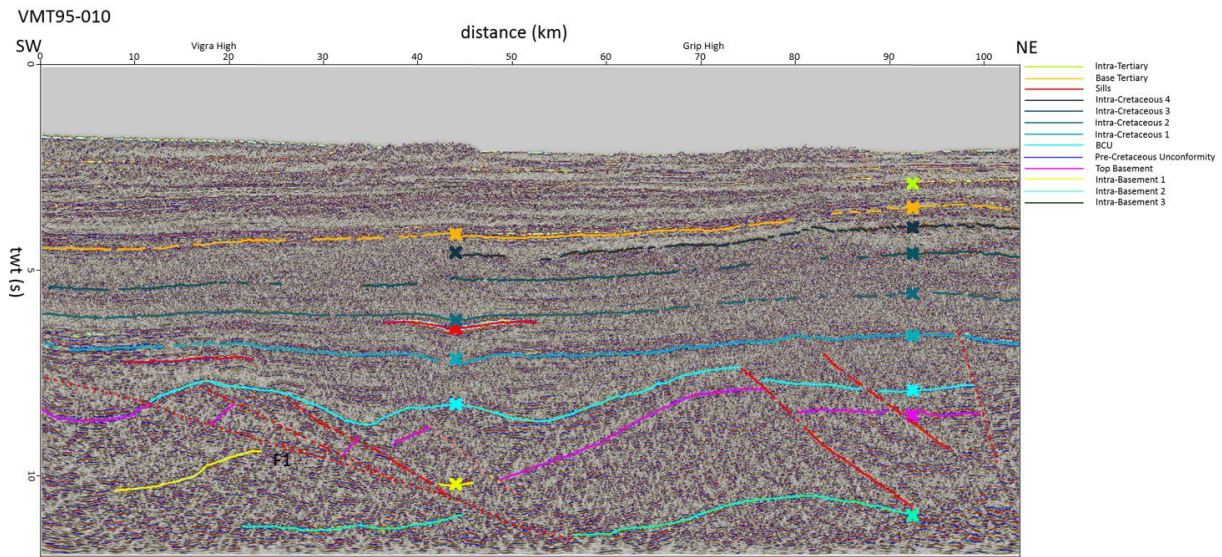

Figure 4.10: Seismic interpretation of VMT95-010

4.10.3   Top Basement and Intra-Basement Reflector

Below the Base Cretaceous, a flat-lying reflector near 8 s twt in the northeast of Grip High is recognized as the top seismic basement according to the interpretation of VMT95-005. In the southwest of Grip High, the top seismic basement is placed at the base of the pre-Cretaceous sedimentary strata. From profile km c. 50 to 0, this area is influenced by F1 and its secondary faults. Based on the northeast dip feature of the faults, some southwest-dipping reflectors in the footwall of these faults are picked and inferred as the top seismic basement. In the footwall of F1, a flat-lying reflector with high amplitude and good continuity near 8 s twt is recognized as the top seismic basement (Figure 4.10).

Below the Top Basement, in the southwest parts of the line, a southwest-dipping reflector with strong amplitude and intermediate continuity is notable, and this reflector can be observed near profile km c. 45 at 10 s twt as well. Considering the discontinuous character of the Middle Crust, we infer it as the Top Middle Crust with some uncertainty (Figure 4.10).

Near 11 s twt, an undulated reflector with high to moderate amplitude and intermediate continuity can be tracked from profile km c. 20 to 90 and is cut by F1. Considering the location of Top Lower Crust in VMT95-004, we infer this reflector as the Top Lower Crust. This inference is of great uncertainty, especially in the footwall of F1 due to the boundary effect in seismic data processing (Figure 4.10).
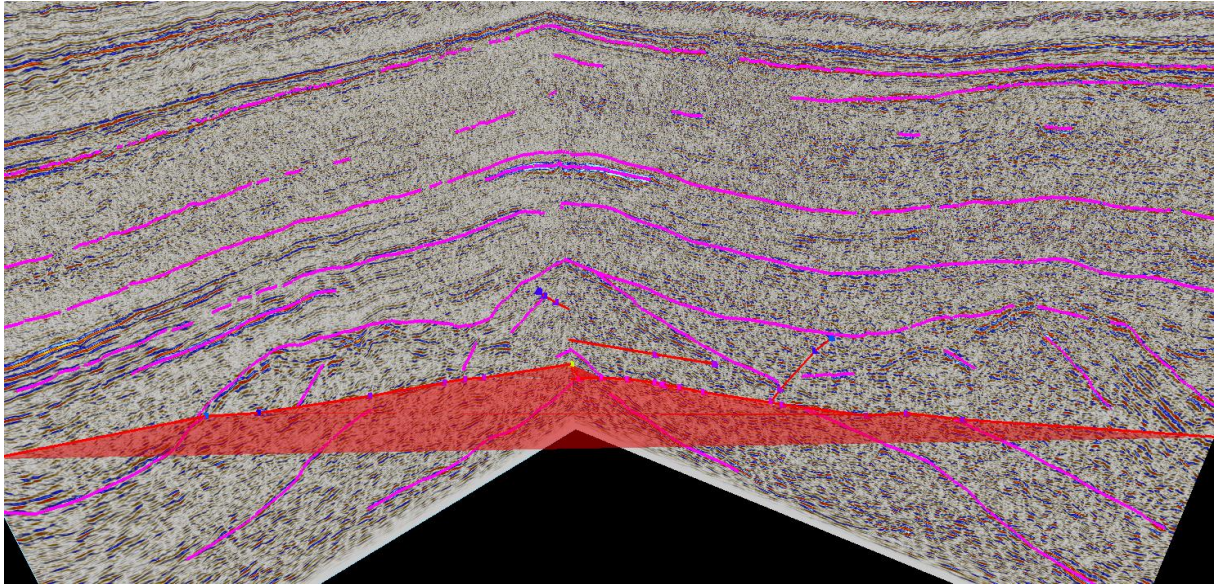
Figure 4.10.1: Fault connection in 3D window

4.10.4 Important Faults

In the 3D window, we find some faults connecting with the faults in VMT95-004 and VMT95-005. Notably, the large-scale low-angle detachment F1 is connecting with the fault below the Vigra High, constituting the fault plane (shown in Figure 4.10.1). This low-angle detachment fault incises into the Lower Crust and thinned the Crust to a great degree. In VMT95-004, it seems to have incised into mantle and lead to mantle exhumation.

4.11 VMT95-011

The VMT95-011 is a NE-SW trend line and located in the southwestern boundary of Møre Basin, perpendicular to the VMT95-001. The southwestern parts of the line goes through the Manet Ridge, Magnus Basin and Magnus Ridge.

4.11.1 From Seabed to BCU

Comparing with VMT95-001, the Base Tertiary and four intra-Cretaceous reflectors are picked and tracked throughout the line. In the Northeast of the line, a largescale normal fault creates a huge deposition accommodation for Cretaceous sediments. Below the intra-Cretaceous 1 reflector, several reflectors with high amplitude and good continuity can be observed, the exact geological age of these reflectors are not likely to be verified due to the lack of well data in this deep basin area. In the northeast of the line, some reflectors with a high amplitude near 5 s twt are interpreted as the sills (Figure 4.11).

Figure 4.11: Seismic interpretation of VMT95-011

4.11.2 BCU

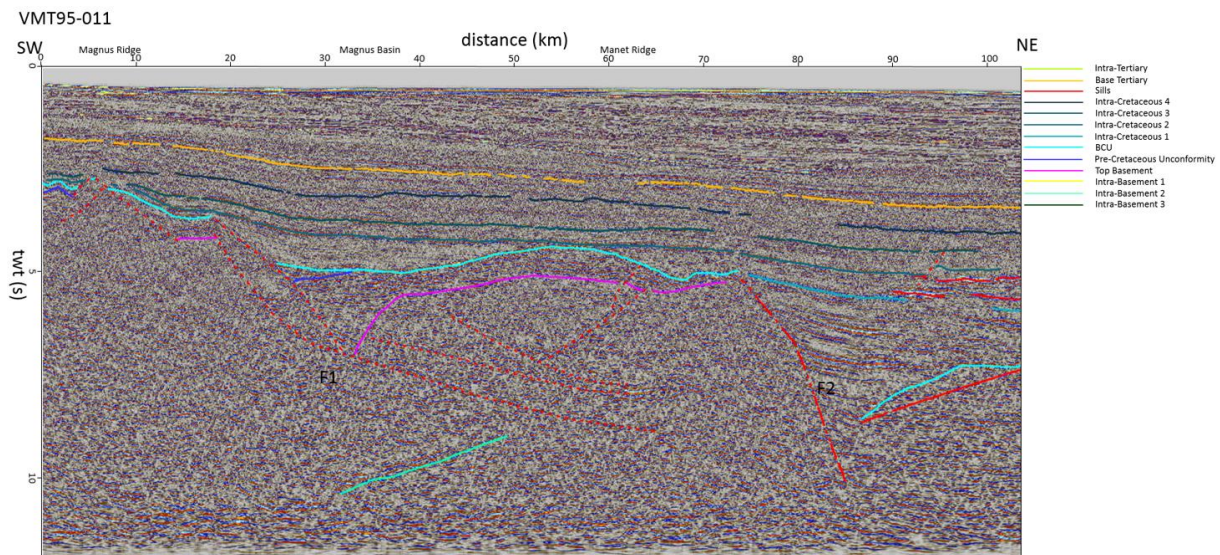In the northeast parts of the line, it is obvious that some reflectors with good continuity and high amplitude in the deep basin terminate at a southwest-dipping reflector. Based on this feature, we infer the south-dipping reflector as the Base Cretaceous Unconformity. From profile km c. 75-10, the Base Cretaceous is onlapped by the parallel Cretaceous sedimentary rocks and is recognized as the Base Cretaceous Unconformity. In the southwest of the Magnus Ridge, two unconformities are recognized near 3 s twt, we infer the upper one as the Base Cretaceous Unconformity (Figure 4.11).

4.11.3 Top Basement and Intra-Basement Reflector

In the northeast of line, the activity of F2 creates a deep sedimentary subbasin. In this deep subbasin, no possible Top Basement reflector can be identified. From profile km c. 75 to 30, the top seismic basement is placed at the base of parallel facies pre-Cretaceous sedimentary strata. In the Magnus Basin, the top seismic basement is onlapped by the pre-Cretaceous sediments, showing an contact relationship of nonconformity. In the southwest of the Magnus Basin, the top seismic basement is placed at the base of pre-Cretaceous strata near 4 s twt, bounded by two normal faults in the northeast and southwest respetively (Figure 4.11).

In the footwall of F1, a reflector with high amplitude and moderated continuity rises northeastwards and is inferred as the Top Lower Crust.

4.11.4 Important Faults

In the northeast deep basin, we identified two faults F2 and F3, and in the 3D window these two faults are inferred to connect with the faults in VMT95-001 (shown in Figure 4.11.1). In the 3D window, it is clear that F2 results in a huge increase for the thickness of Cretaceous sedimentary strata, which means the crust is thinned to a large degree here.
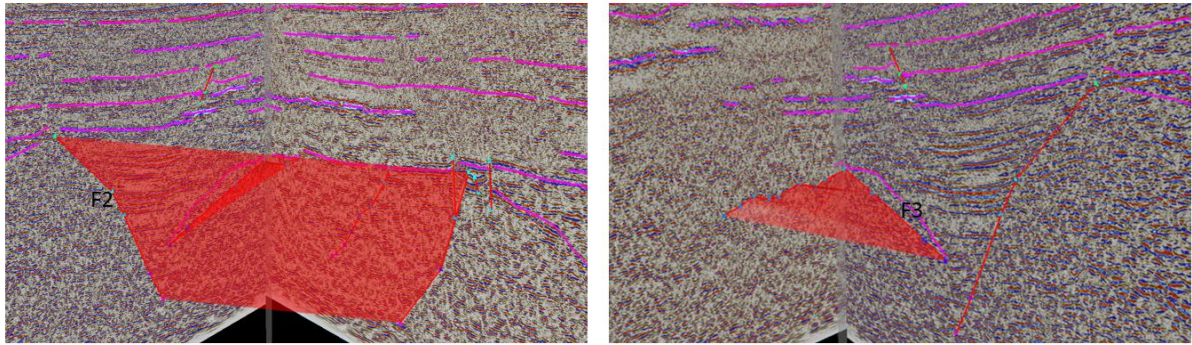
Figure 4.11.1: Fault connection in 3D window

In the Magnus Basin, a southwest-dipping angular unconformity is onlapped small wedge-shaped syn-rift sedimentary strata cut by a moderate normal fault which connects with F1 and could be the secondary fault of F1. We infer that the sedimentary strata above the pre-Cretaceous unconformity is the syn-tectonic deposition of the secondary normal fault.

In the hanging wall of F1, two low angle northeast-dipping moderate faults are recognized and inferred as the secondary faults of F1, though it seems these two faults don't connect with F1. Due to lack of seismic lines perpendicular to the VMT95-011 in the southwestern parts of the line, the 3D connection of these two faults and F1 cannot be shown.

4.12 Time Depth Conversion

The raw seismic lines are performed in time domain, in order to know the depth of key horizons, such as the Top Basement and Moho. The interpreted seismic lines have to be converted to depth domain. In this study, we choose four representative lines, including VMT95-004, VMT95-006, VMT95-007 and VMT95-008, to converted into depth domain.

The first step in time-depth conversion is to create a velocity model which acts as the input for conversion. In this study, we choose the velocity published by Mjelde et al. (2009), whose study is also located in the More Basin and near the chosen seismic lines. Based on his velocity model, the average values used in this study are derived according the different thickness of the layers (shown in Table 3). We use the function of General Domain Conversion in Petrel. For the function, major horizons have been defined and the velocity values have been assigned to the different layers. The surfaces have been defined in the time domain and average velocities have been defined for each layer. The result is shown in Figure 4.12 and 4.13.

Layer	P-wave velocity [km/s] (Mjelde et al., 2009, profile 2-99)	Velocity values used in this study [km/s]
Seabed - Base Tertiary	1.8-2.1	2.0
Base Tertiary – Base Cretaceous	2.8-5.2	4.0
Base Cretaceous – Top Basement	5.3	5.3
Top Basement – Top Lower Crust	6.2	6.2
Top Lower Crust - Moho	6.7	6.7

Table 3: The values of P-velocity derived from the modelling of OBS data published by Mjelde et al. (2009) and velocity values used in this study
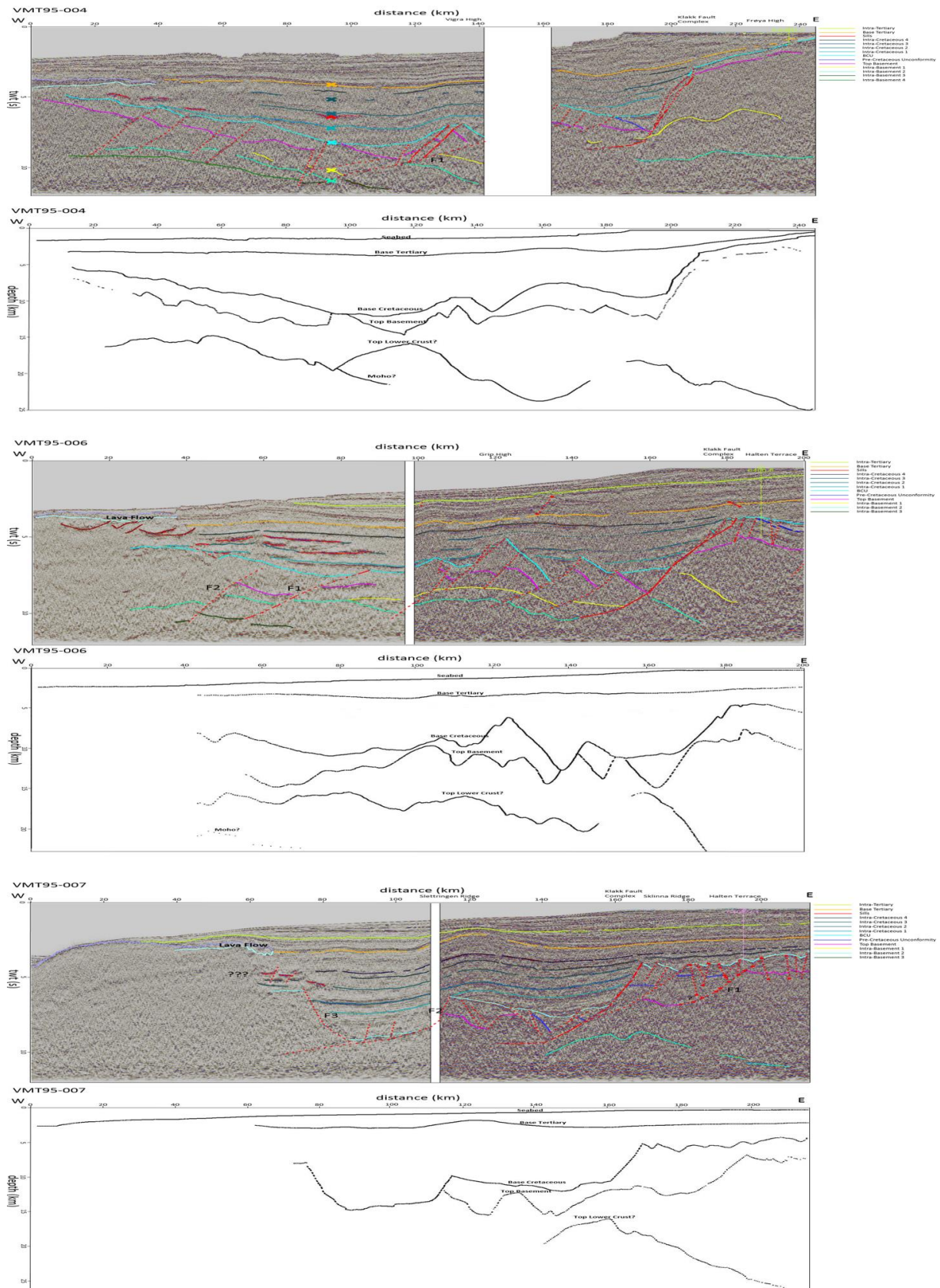
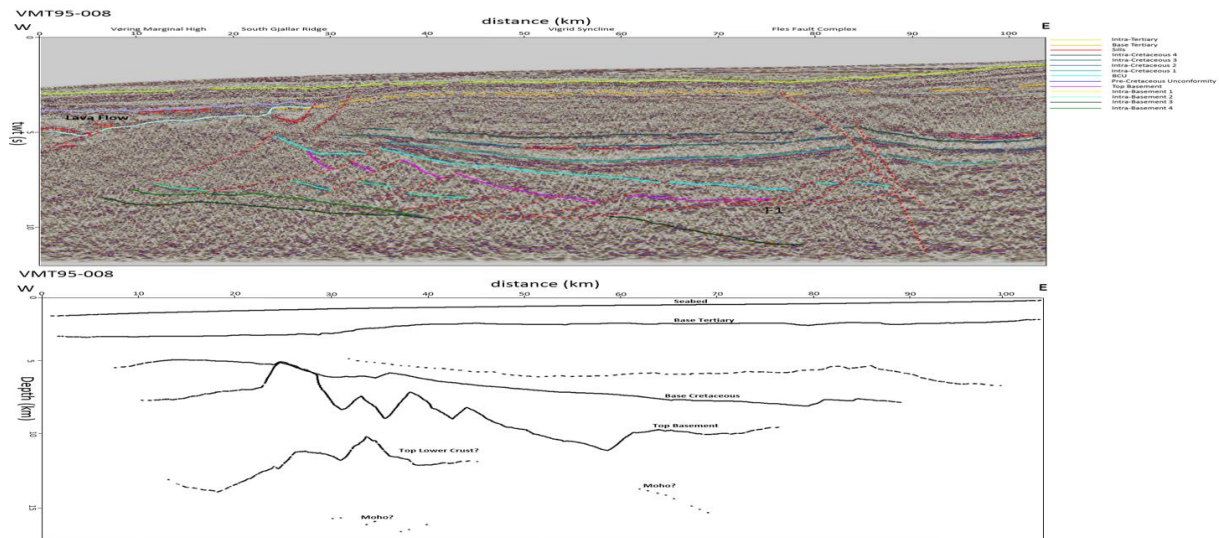Figure 4.12: Time depth conversion result of VMT95-004, 006, and 007

Figure 4.13: Time depth conversion result of VMT95-008

In VMT95-004, we can observe that the crust is thinned to about 6 km near profile km c. 110 from more than 20 km in the easternmost of the line, caused by a series west-dipping normal faults especially the detachment fault F1. And the inferred Moho rises to 20 km and is considered to be cut by F1. In VMT95-006, from profile km c. 90 to 50, the Top Basement goes down quickly, and inferred Moho rises to 20 km, the crust thinning here is also considerable. In VMT95-007, the depth of Base Cretaceous is 15 km from profile km c. 110 to 90, indicating a dramatical crust thinning here. And the Top Basement cannot be observed in the reflective seismic, we infer that the upper crust or even the lower crust is moved to another place by the detachment F2, resulting in extension allochthons in the hanging wall of F2. Due to influence by the overlying lava flow, the extension allochthons cannot be clearly observed. This area has a high possibility of mantle exhumation. In VMT95-008, we infer two reflectors as Moho, considering the 15 km depth of these two reflectors after a dramatical crust thinning by detachment F1. Near profile km c. 70, the crust is thinned to about 4 km by F1. In these four seismic lines, the depth of Top Basement can reach to about 15 km, which coincide well with the work of Ebbing & Olesen (2010) who presented the first complete top basemen map for the passive margin system of the Norwegian continental shelf based on the potential field data. In the most of the lines in the study area, we can hardly find the possible Moho, possibly caused by that the time domain maximum is 12 s which is a little small for Moho. In the VMT95-004, we observe that the crust is thinned to about 6 km near profile km c. 110, this value is different with the work of Ebbing & Olesen (2010). We give two possible explanations. The first one is that the inferred Moho in VMT95-004 is located near the bottom of the seismic image and it might be the interface of the altered mantle and lower crust, the real Moho is below this reflector and located outside the seismic image. The second one is that the area where the crust is thinned to about 6 km only has a length of less than 20 km, in other words this anomaly may be too small, and the resolution of potential field data is not good enough to detect this small anomaly. In VMT95-006 and 008, the depth of inferred Moho can match the work of Ebbing & Olesen (2010) well.

5 Result and Discussion

5.1 Domain Subdivision and Fault Breakaway Complex Classification

In the previous work, different geophysical methods have been used to study the deep structure of the Mid-Norwegian margin. Péron-Pinvidic et al. (2013) compare the magma-poor Iberia-Newfoundland, the magma-rich mid-Norway-East Greenland and the sediment-rich Angola-Brazil rifted margins and suggest that magma-rich systems may go through a stage of hyper-extension. Osmundsen et al. (2016) favour a model where mantle windows were exhumed in the footwall of some of the master faults in the Cretaceous, based on a process-oriented evaluation of the different interpretation scenarios of 6 crustal transects. Nirrengarten et al. (2014) proposed that their seismic, magnetic and gravity data does not easily support large scale exhumation of serpentinized mantle in the inner and is unlikely in the outer parts of the Møre Basin based on the analysis of three transects in Møre Basin. Zastrozhnov et al. (2020) also hold the similar views that their observations do not support evidence for a large zone of exhumed upper mantle based on the analysis of 8 transects in Møre an Vøring Basin.

In this study, based on the terminology proposed by Péron-Pinvidic et al. (2013) and Osmundsen & Péron-Pinvidic (2018), some faults in the seismic lines have been classified to different breakaway complexes. The inner necking breakaway complex is normally associated with an abrupt but moderate increase in deposition accommodation. According to this feature, the F1 with an accurate named Vingleia Fault Complex in VMT95-005 is identified as the inner breakaway complex. In VMT95-003, The Slørebotn detachment in the easternmost of the line also has this kind of feature to a certain extent. The outer necking breakaway complex is characterized by a very large accommodation increase and high-β normal fault type 1 (shown in Figure 2.7d). Based on this feature, the outer necking breakaway complex is recognized in most of the lines and the Møre-Trøndelag Fault Complex and Klakk Fault Complex are classified into outer necking breakaway complex. The distal breakaway complex is associated with tectonic unroofing and extensional allochthons. Based on it, we recognize the distal breakaway complex in VMT95-004, 007, 008 and probably 002 as well. Notably in VMT95-007, in the hanging wall of F2, the depth of sediments can reach to 15 km, and below F2, we cannot find any possible reflectors of basement, which means this area is moved a more distal place according to the seismic reflection data. Thus, F2 is considered as the distal breakaway complex. In VMT95-002, we have also found this kind of fault: the northwest bounding fault of the South Vigra High. In northwest of the Vigra High, the depth of sediments can reach to 10 s twt and the upper crust is thinned to a large degree. Thus, we classify this fault as the distal breakaway complex with some uncertainty that the seismic signal in the northwest parts of the line is not that good due to the overlying lava flow. In VMT95-008, the thickness of basement in the hanging wall of F1 from profile km c. 70 to 80 is less than 0.5 s twt, giving an evidence that the crust is extremely highly thinned here. Thus, we classify the F1 as part of distal breakaway complex. And in VMT95-004, we also find this feature near profile km c. 120, and it is clear that extension allochthon is located in the hanging wall of F1 (Figure 5.1 and 5.2).

As mentioned above, the inner necking and outer necking breakaway complex are the important boundaries for proximal, necking and distal domain. Based on it, we finished the subdivision of domain (shown in the Figure 5.1 and 5.2). In Figure 5.3, we draw a schematic map showing subdivision of the study area into domains bounded by major breakaway fault complexes based on the structural-element map from NPD[1].
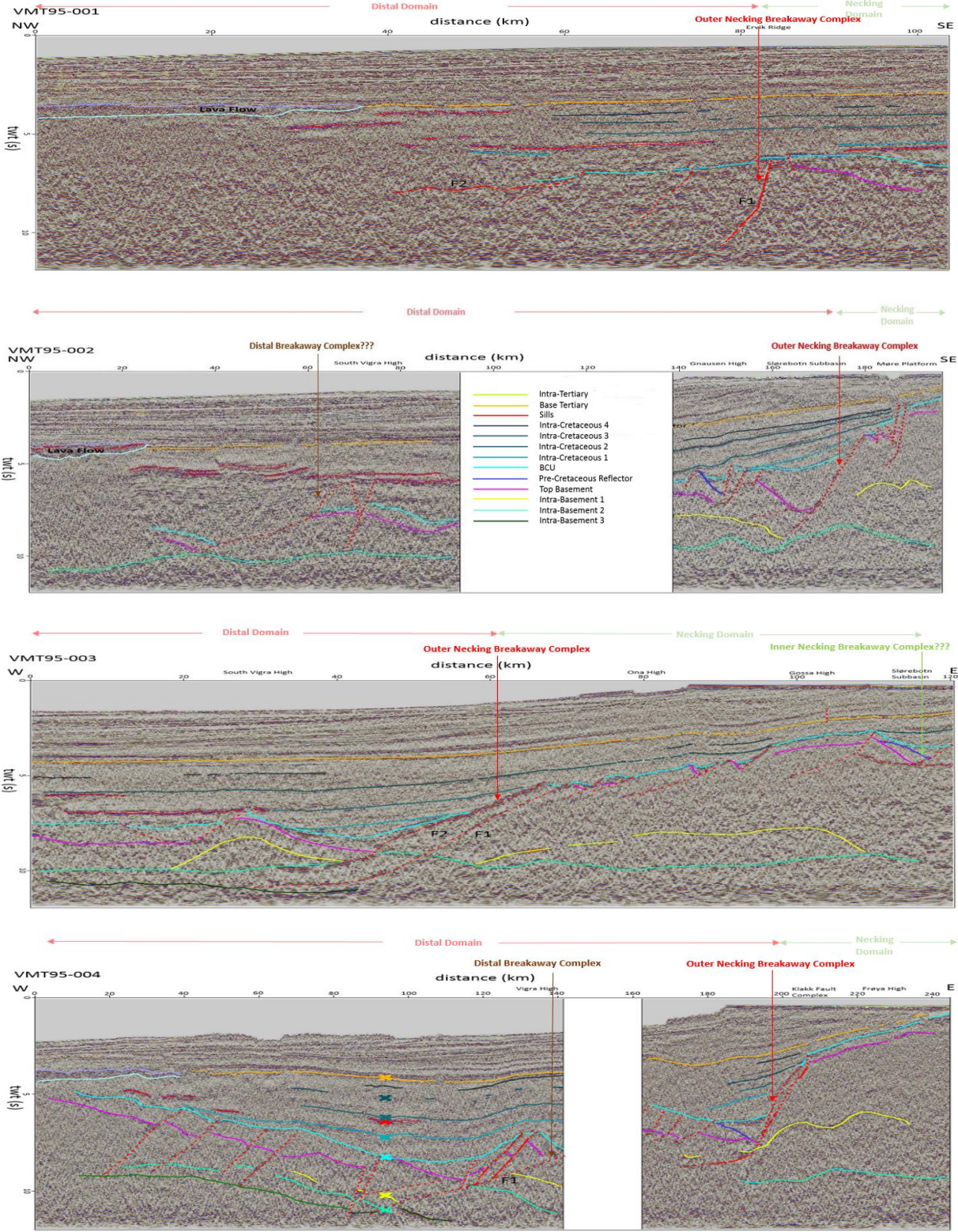

Figure 5.1: Domain subdivision and classification of fault in the seismic lines (VMT95-001, 002, 003 and 004)
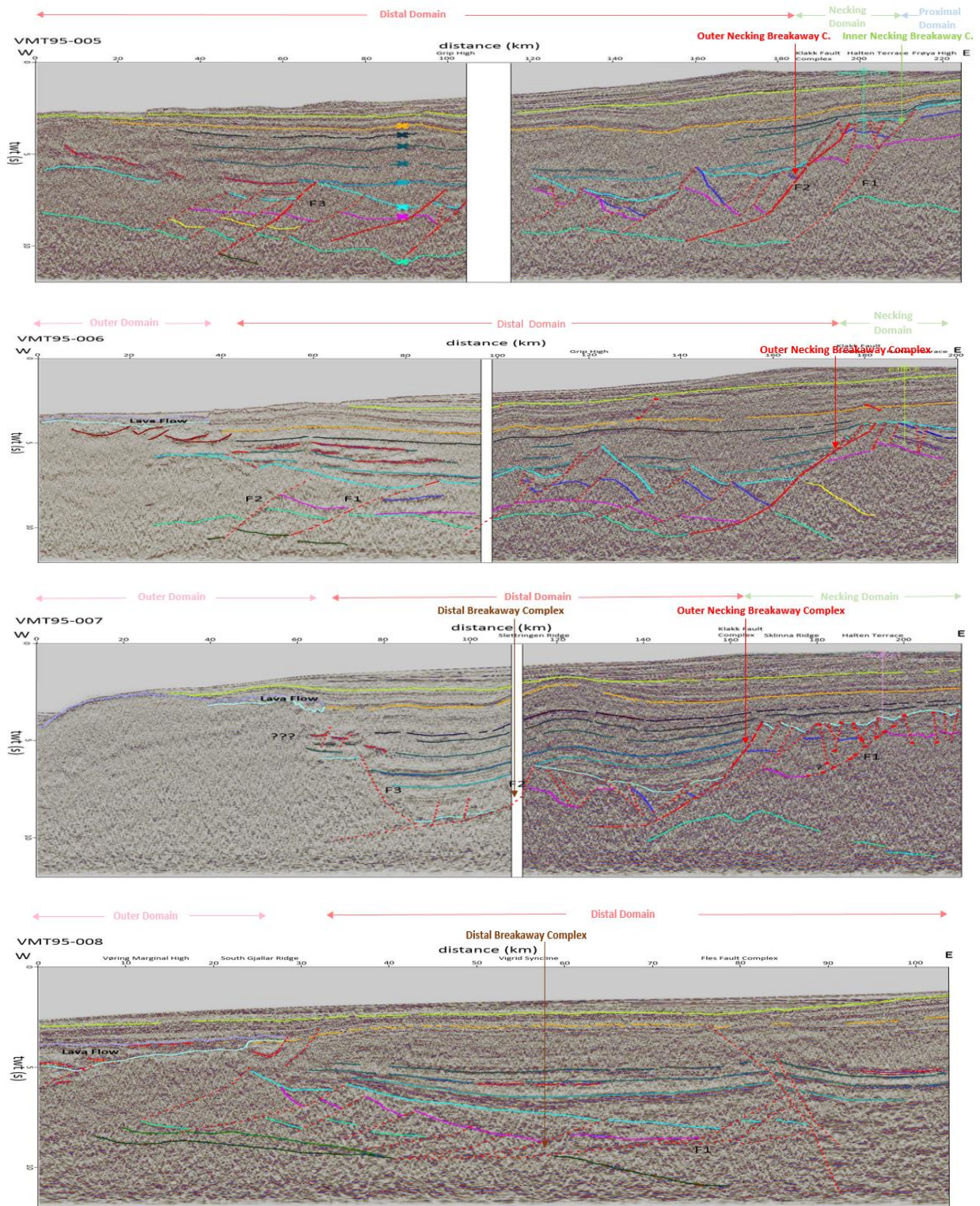
Figure 5.2: Domain subdivision and classification of fault in the seismic lines (VMT95-005, 006, 007 and 008)
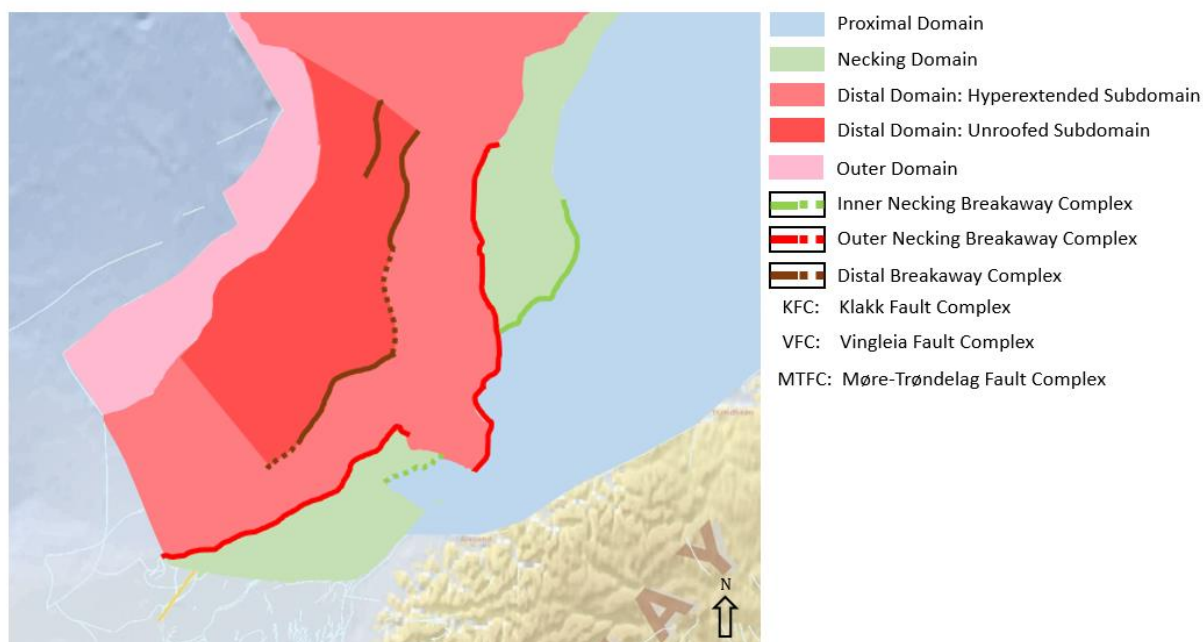
Figure 5.3: Domain subdivision of the study area based on the major breakaway complex and seismic interpretation

In the southeast of the MTFC, we divide the area into necking domain based on that the outer necking breakaway complex is the boundary of necking domain and distal domain. However, due to the lack of seismic lines in this area, the inner boundary of necking domain is of high uncertainty. In VMT95-002, the southeast bounding fault of Slørebotn Subbasin is classified as the outer necking complex, which may have some collision with the MTFC which is recognized as the outer necking complex as well. And in this line, the distal breakaway is marked as dotted line due to the uncertainty mentioned above. In the VMT95-003, we think the Slørebotn detachment could be classified into the inner necking breakaway complex but due lack of seismic data in the eastern of Slørebotn detachment, thus, we use dotted line to represent it. As the distal breakaway complex is the boundary of hyperextended and unroofed area, we subdivide the distal domain into two subdomains: hyperextended and unroofed domain. In VMT95-006 and 007, we cannot find the distal breakaway complex based on the reflection seismic data. So, we use dotted line to represent an inferred position in Figure 5.3. And in the north of the study area, due to the lack of W-E trend seismic lines, we can't subdivide the distal domain into subdomains. From Figure 5.3, we can infer that at least some parts of distal margin have experienced tectonic unroofing and mantle exhumation may happen in these area.

5.2 Comparison with South China Sea

The South China Sea (SCS), the largest marginal sea in the western Pacific region, developed as the result of the Cenozoic rifting and seafloor spreading of the South China margin (Qing et al., 2018). Same as the NE Atlantic, it has experienced several rifting stages, crustal breakup, seafloor spreading. In these two passive margins, great amounts of normal faults are formed in different stages and control the deposition in the subbasin area, several important unconformities can be observed and separate the different stage sediments.

Since the 1990s, the tectonic evolution of South China Sea has been heatedly debated. To explain the opening of South China Sea, two major models, including collision-extrusion model shown in Figure 5.4A (Briais et al., 1993; Replumaz & Tappomnier, 2003) and subduction-collision model shown in Figure 5.4B (Holloway, 1982; Hall, 2002; Pubellier & Morley, 2014), have been proposed. Pinxian et al. (2019) proposed another different model (shown in Figure 5.4C): the SCS was separated from the Eurasian continent along strike-slip faults inherited from the Late Mesozoic, followed by lithospheric stretching along the
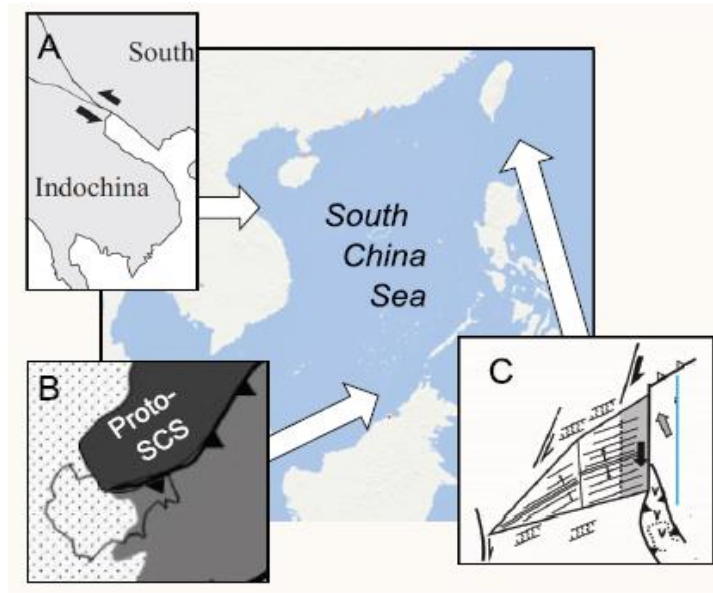

Figure 5.4: Three models for the opening of South China Sea (Pinxian et al., 2019)

Eurasian/Huatung Plate boundary in the Early Cenozoic. In these three model for opening of South China Sea, we can find a similarity that the Eurasian plate stay relatively static, which means the opening space of South China Sea is limited and South China Sea can only open southwards or southwestwards.

What is agreed by most people is that based on the stratigraphy study, the rifting history of South China Sea can date back to the Late Cretaceous and be divided into three stages. The first stage is from the Latest Cretaceous to Early Paleocene when a Mesozoic convergent margin changed to extension. The second one is from the Late Paleocene to Eocene which is markable by N-S extension and observed in nearly all offshore basins. The third one is from the Late Eocene to Early Miocene which resulted subsequently in seafloor spreading in the South China Sea (Franke et al., 2014). The final breakup of the eastern subbasin occurred in the Early Oligocene, then the ridge jumped to the south. The breakup of the southwestern subbasin occurred in the Late Oligocene about 25 Ma. Seafloor spreading ceased about 10-15 Ma, the collision between the Australia and Asian plates caused the rotation of Borneo and the closure at the south boundary of the South China Sea.

Franke et al. (2014) interpreted some seismic reflection profiles across the South China Sea, including two lines across the eastern subbasin and southwestern subbasin (shown in Figure 5.5). Comparing these two subbasins gives insight into crustal configuration in two rift settings: (1) Magma-poor rifted margins at the transition to the seafloor spreading stage and (2) magma-poor margins deformed by additional extension at the tip of the propagator. He suggests that most bounding faults sole out within the middle crust and only normal faults within about 50 km from COT is considered to reach the mantle.

Comparing these two sections to the study area, we can find three major differences between the South China Sea and Mid-Norwegian margin.

Firstly, in both two sections, an unusual undulation of Moho in the proximal domain can be observed: Xisha Trough and Baiyun Sag. In these two sag basins, the crust is thinned to a large extent and the syn-rift sediments is much thicker than other areas. Zhichao et al. (2018) interpreted a deep seismic reflection profile across the Baiyun Sag (shown in Figure 5.6b). In his interpretation, a northwest-dipping detachment fault results in the highly-
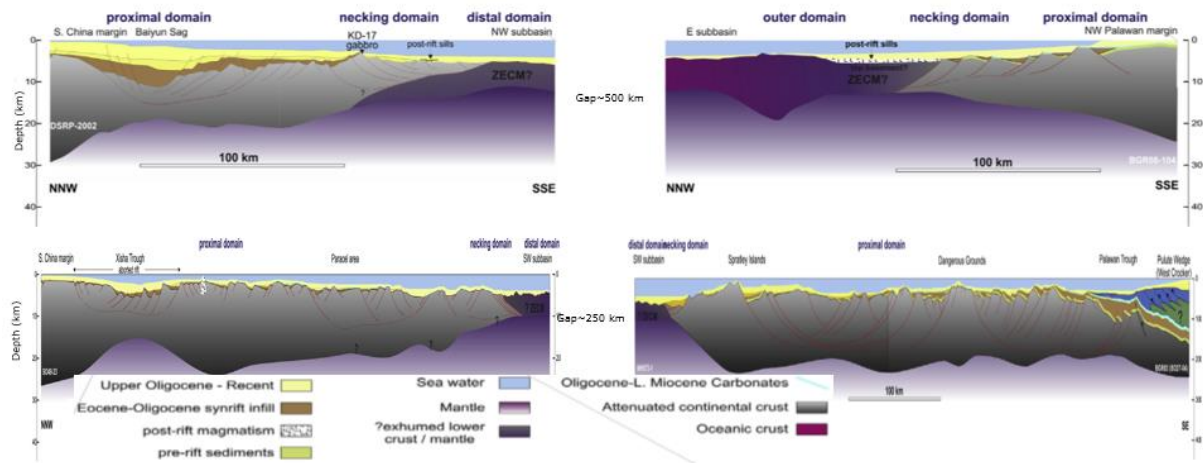

Figure 5.5: Crustal-scale section across the eastern and southwest subbasins from up to down respectively (Franke et al., 2014)

thinned crust and this detachment fault is considered to incise into the mantle. Linlong et al. (2018) proposed that the central part of the Baiyun sag is a more evolved rift center in the necking domain that became abandoned during rifting and that further extension became localized in the more distal margin. Similarly, the Xisha Trough is also considered as a failed continental breakup by Sibuet al. (2016). After the onset of oceanic crust at 33 Ma, the propagation of the seafloor spreading extended in the NW east sub-basin but not in the Xisha trough where rifting still occurred, with a transform fault continuing to survive between the east and NW east sub-basins. The Xisha trough is a failed rift arm that recorded thinning of the continental crust from~25 km to 8 km, opened during the Early Oligocene and whose motion is transformed along the Qui Nhon ridge, located in the prolongation of the Red River fault system. Chao & Jianye (2016) interpreted a seismic line across the Xisha Trough (shown in Figure 5.6a). In his interpretation, it is clear that the crust here is thinned to a large degree and some normal faults have incised into the mantle. In the Mid-Norwegian margin, we cannot find this kind of highly-thinned area in the proximal and necking domain based on the previous study. In the East Greenland margin, Jameson Land basin is considered as the aborted inner rift basin by Péron-Pinvidic et al. (2013).
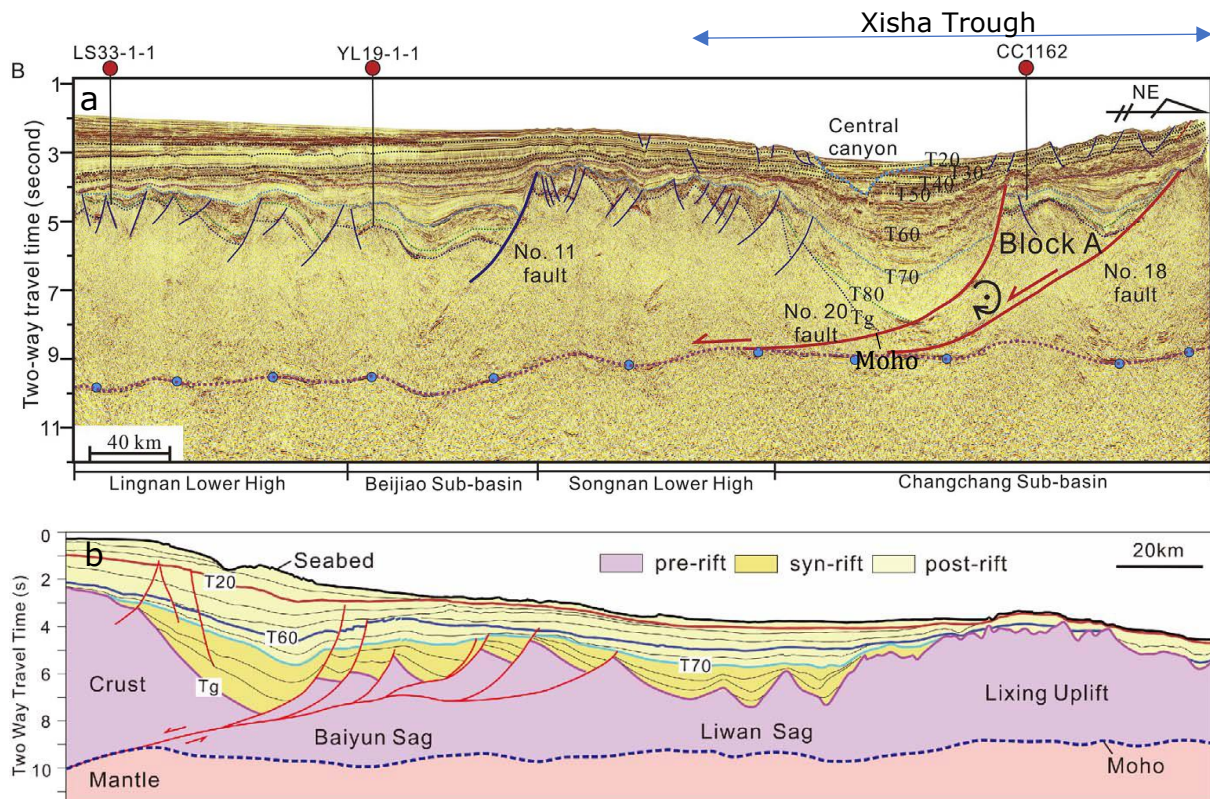
Figure 5.6: Deep seismic reflection profile across the Eastern Segment of the Xisha Trough and Baiyun Sag (Chao & Jianye, 2016; Zhichao et al., 2018)

Another notable difference between the Mid-Norwegian margin and South China Sea is the distal domain. In the Mid-Norwegian margin, the outer necking breakaway complex is the boundary that separates the necking domain and distal domain. A distinct feature of outer necking breakaway complex is a very large accommodation increase in its hanging wall and it is the first fault that cuts into the middle crust and continues into the lower crust, even upper mantle. The outer necking breakaway complex can be found in all seismic profiles in the study area and can be regarded as a typical feature of the Mid-Norwegian margin. In the South China Sea, we find that only a landward dipping fault near the Spratly Islands has created a distinct accommodation increase for syn-rift sediments and cut into deep parts of crust, except two special sag basins. In the southeast parts of South China Sea, the seismic survey is much less than that in the northwest parts of South China Sea, more geophysical works, especially reflective seismic, in the future may contribute to some new findings.

Another important feature of distal domain in Mid-Norwegian margin is the distal breakaway complex. In the Mid-Norwegian margin, it marks the inner boundary for an area of potential major tectonic unroofing, and if extension was sufficient, mantle exhumation (Osmundsen & Péron-Pinvidic, 2018). In the study area, we can observe that some low-angle detachment faults cut into the lower crust and even mantle and extensional allochthons lie on the top of detachment surface, such as the distal breakaway complex in VMT95-004 and VMT95-008, or the depth of sedimentary rocks is pretty large, for example the depth of Base Cretaceous in VMT95-007 is about 15 km, which also indicates that the crust is thinned to a large degree by the normal faults, such as the distal breakaway complex in VMT95-002 and VMT95-007. In South China Sea, the distal domain is poorly defined. The breakaway terminology seems not able to work here due to the narrow distal

domain possibly caused by lacking hyperextension. We cannot find this kind of detachment fault incising into the lower crust and even mantle and obvious extension allochthons in the hanging wall of detachment in the distal domain. We infer that the South China Sea may not go through a stage of hyper-extension as Mid-Norwegian margin, except some aborted sag basins, such as Baiyun Sag and Xisha Trough. This may result from different nature of lithosphere, rifting duration and the movement of related plates. Pinxian et al. (2019) proposed to discriminate two types of rifting basins: plate-edge type such as the South China Sea and intra-plate type like the Atlantic. The two types of continent rifting occur at two different stages in the Wilson cycle. Intra-plate rifting occurs at an early stage in the Wilson cycle and is associated with continental break-up, whereas the plate-edge rifting takes place much later. Thus, the two types of rifted basins differ from each other not only in structure and formation process, but also in their lifespan and geographic size. As a member of the Western Pacific system of marginal seas, the South China Sea should be studied not in isolation on its origin and evolution, but in a systematic context to include also its neighboring counterparts, such as Sea of Japan, Gulf of California, Lau Basin and Woodlark Basin.

Thirdly, based on the four time-depth converted seismic lines in the Mid-Norwegian margin, we find that the depth of top basement is between 10 and 15 km in the deep basin area. In the South China Sea, the depth of top basement is less than 10 km in the distal margin area based on the sections from Franke et al. (2014) and Savva et al. (2014). Braitenberg et al. (2006) drew the map of top basement based on the gravity data (shown in Figure 5.7a). In Figure 5.7a, we can observe that the depth of top basement is less than 5 km in the most of area located outside the continental-ocean boundary, and inside the continental-ocean boundary it ranges from 3 to 10 km. The depth of top basement in the
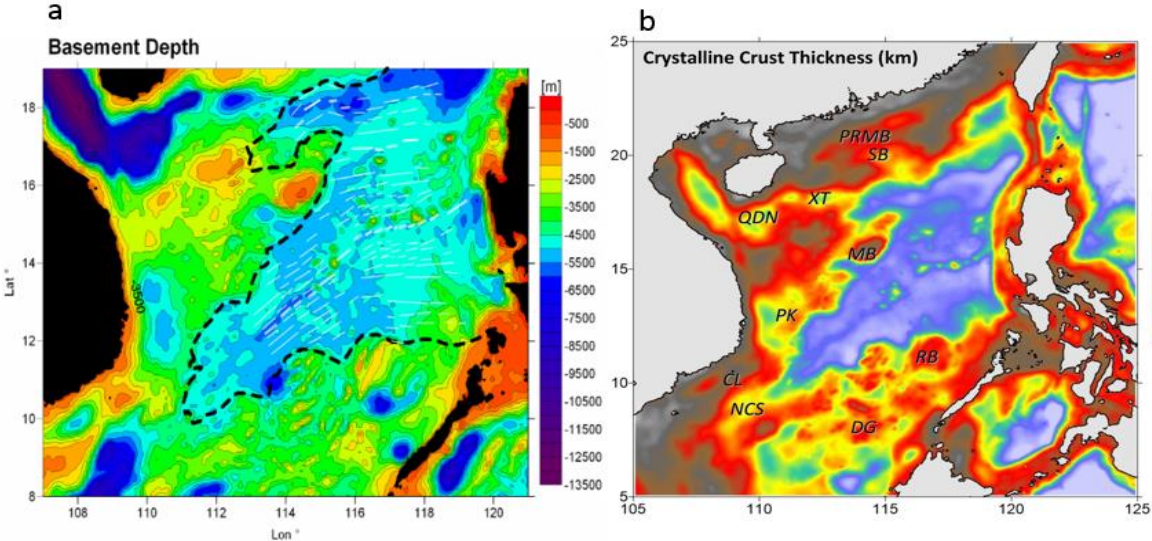
Figure 5.7: The depth of top basement (a) and the crystalline crust thickness (b) in the South China Sea, the dotted line represents the continental-ocean boundary (Braitenberg et al., 2006; Gozzard et al., 2018)

South China Sea is obviously smaller than that in the Mid-Norwegian Margin. In Figure 5.7b, Gozzard et al. (2018) used the inversion of satellite-derived free-air gravity-anomaly data to map crustal thickness in the South China Sea. We can observe that the crystalline crust thickness is almost near 0 km inside the continental-ocean boundary, and outside the continental-ocean boundary it is more than 15 km in the most area. In VMT95-004 and 008, the crust is thinned to near 5 km in the distal domain, caused by the low-angle

detachment faults. Comparing the thickness of crystalline crust in the South China Sea and Mid-Norwegian margin, we suggest again that the South China Sea may not go through a stage of hyper-extension as Mid-Norwegian margin.

6 Conclusion

We have interpreted selected horizons in 11 long seismic reflective profiles, the selected horizons, such as Base Cretaceous, Base Tertiary and Top Basement, and main fault structures have been picked. These interpretations show the results of different stages of rifting, thus are important to understand the rifting process of Mid-Norwegian Margin. Based on the interpretation, we divide the margin area into different domains and some breakaway complexes are also classified. Finally, we picked two typical seismic sections of South China Sea and compare it with the Mid-Norwegian Margin. The main conclusions can be summarized as follows:

1. A typical feature for all the seismic lines in Mid-Norwegian margin is that the outer necking domain complex, which is the boundary for the necking domain and distal domain. An enormous accommodation increase created by the outer necking breakaway complex can be observed in all seismic lines. We infer that the outer necking breakaway complex is active throughout all the extension stages or is reactivated at a certain stage and continues to be active until the final breakup.
2. Based on the depth-converted lines, we can find that the crust is thinned to a dramatical degree in the distal domain of the study area, especially in VMT-008 the thickness of the crust is less than 5 km. We suggest that mantle exhumation may have occurred in VMT95-004 and VMT95-008, as well as VMT95-007 with a smaller possibility.
3. In the South China Sea, the distal domain is very narrow and the distal breakaway complex, which is the inner boundary for an area of potential major tectonic unroofing, cannot be observed, except two sag basins: Xisha Trough and Baiyun Sag, which are considered as the failed rifting. Comparing the thickness of crystalline crust in the South China Sea and Mid-Norwegian margin, we suggest that the South China Sea may not go through a stage of hyper-extension as Mid-Norwegian Margin, possibly resulting from the different nature of lithosphere, short rifting duration and movement of nearby plate, especially the Australian plate.

References

Blystad, P., Brekke, H., Farseth, R. B., Larsen, B. T., Skogseid, J. & Tørudbakken, B. 1995, Structural elements of the Norwegian continental shelf. Norwegian Petroleum Directorate Bulletin, 8.

Brekke, H., Sjulstad, H.I., Magnus, C., Williams, R.W., 2001. Sedimentary environments offshore Norway - an overview, in Sedimentary environments offshore Norway–Palaeozoic to Recent, 10, 7-37, eds. Martinsen, O.J. and Dreyer, T., Elsevier Science B.V., Amsterdam.

Briais, A., Patriat, P., Tapponnier, P., 1993. Updated interpretation of magnetic anomalies and seafloor spreading stages in the South China Sea: implications for the tertiary tectonics of Southeast Asia. Journal of Geophysical Research. 98 (B4), 6299-6328.

Braitenberg, C., Wienecke, S., and Wang, Y. (2006), Basement structures from satellite-derived gravity field: South China Sea ridge, J. Geophys. Res., 111, B05407, doi:10.1029/2005JB003938.

Chao Lei, Jianye Ren, 2016. Hyper-extended rift systems in the Xisha Trough, northwestern South China Sea: Implications for extreme crustal thinning ahead of a propagating ocean. Marine and Petroleum Geology, 77, 846-864.

Dieter Franke, Dimitri Savva, Manuel Pubellier, Stephan Steuer, Benoit Mouly, Jean-Luc Auxietre, Florian Meresse, Nicolas Chamot-Rooke, 2014. The final rifting evolution in the South China Sea. Marine and Petroleum Geology, 58 (B), 704-720.

Dmitry Zastrozhnov, Laurent Gernigon, Iakov Gogin, Sverre Planke, Mansour M. Abdelmalak, Stéphane Polteau, Jan Inge Faleide, Ben Manton, Reidun Myklebust, 2020. Regional structure and polyphased Cretaceous-Paleocene rift and basin development of the mid-Norwegian volcanic passive margin. Marine and Petroleum Geology, 115. https://doi.org/10.1016/j.marpetgeo.2020.104269.

Doré, A. G., Lundin, E. R. 1996. Cenozoic compressional structures on the NE Atlantic margin: nature, origin and potential significance for hydrocarbon exploration. Petroleum Geoscience, 2, 299-311.

Doré, A. G., Lundin, E. R., Fichler, C. & Olesen, O. 1997b. Patterns of basement structure and reactivation along the NE Atlantic margin. Journal of the Geological Society 154, 85-92.

Doré, A. G., Lundin, E. R., Jensen, L. N., Birkeland, Ø., Eliassen, P. E. & Fichler, C. 1999. Principal tectonic events in the evolution of the northwest European Atlantic margin. In: Petroleum Geology of Northwest Europe: Proceedings of the 5th Conference (edited by Fleet, A. J. & Boldy, S. A. R.). Geological Society, London, 41–61.

Driscoll, N. W., Hogg, J. R., Christie-Blick, N. & Karner, G. D, 1995. Extensional tectonics in the Jeanne D'Arc Basin, offshore Newfoundland: implications for the timing of break-up between the Grand Banks and Iberia. Geological Society, London, Special Publications, 90, 1-28.

D. Savva, M. Pubellier, D. Franke, N. Chamot-Rooke, F. Meresse, S. Steuer, J.L. Auxietre, 2014. Different expressions of rifting on the South China Sea margins. Marine and Petroleum Geology. 58 (B), 579-598.

Ebbing, J., Olesen, O., 2010. New compilation of top basement and basement thickness for the Norwegian continental shelf reveals the segmentation of the passive margin system. Geological Society, London, Petroleum Geology Conference series, 7, 885-897. https://doi.org/10.1144/0070885

Færseth, R. B., Gabrielsen, R. H. & Hurich, C. A. 1995. Influence of basement in structuring of the North Sea basin, offshore southwest Norway. Norsk Geologisk Tidsskrift 75, 105-119.

Hall, R., 2002. Cenozoic sedimentation and tectonics in Borneo: climatic influences on orogenesis. In: Jones, S., Frostick, L. (Eds.), Sediment Flux to Basins: Causes, Controls and Consequences, vol. 191, pp. 5e22.

Holloway, N., 1982. North Palwan block, Philippines e its relation to Asian mainland and role in evolution of South China Sea. AAPG 66 (9), 1355-1383.

Kallweit R. and L. Wood, 1982. The limits of resolution of zero - phase wavelets. Geophysics, 47. No. 07, 1035-1046.

Jean-Claude Sibuet, Yi-Ching Yeh, Chao-Shing Lee, 2016. Geodynamics of the South China Sea. Tectonophysics. 692 (B), 98-119.

Linlong Yang, Jianye Ren, Kirk McIntosh, Xiong Pang, Chao Lei, Yanghui Zhao, 2018. The structure and evolution of deepwater basins in the distal margin of the northern South China Sea and their implications for the formation of the continental margin. Marine and Petroleum Geology. 92, 234-254. https://doi.org/10.1016/j.marpetgeo.2018.02.032.

Morton, N. 1989. Jurassic sequence stratigraphy in the Hebrides Basin, NW Scotland. Marine and Petroleum Geology, 6, 243-260.

Müller, R., Nystuen, J. P., Eide, F., & Lie, H., 2005. Late Permian to Triassic basin infill history and palaeogeography of the Mid-Norwegian shelf-East Greenland region. In B. Wandås, et al. (Eds.), Onshore-Offshore Relationships on the North Atlantic Margin, Special Publications (Vol. 12, pp. 165–189). Trondheim, Norway: Norwegian Petroleum Society. https://doi.org/10.1016/S0928-8937(05)80048-7.

M. Nirrengarten, L. Gernigon, G. Manatschal, 2014. Lower crustal bodies in the Møre volcanic rifted margin: Geophysical determination and geological implications. Tectonophysics, 636, 143-157. https://doi.org/10.1016/j.tecto.2014.08.004.

Osmundsen, P. T. and Ebbing, J, 2008. Styles of extension offshore mid-Norway and implications for mechanisms of crustal thinning at passive margins, Tectonics, 27, 1-25. https://doi.org/10.1029/2007TC002242.

Osmundsen, Per Terje; Péron-Pinvidic, Gwenn; Ebbing, Jørg; Erratt, Duncan; Fjellanger, Erik; Bergslien, Dag; Syvertsen, Svein Erik. (2016) Extension, hyperextension and mantle exhumation offshore Norway: A discussion based on 6 crustal transects. Norsk Geologisk Tidsskrift. vol. 96 (4).

Osmundsen, P. T., & Péron-Pinvidic, G. (2018). Crustal-scale fault interaction at rifted margins and the formation of domain-bounding breakaway complexes: Insights from offshore Norway. Tectonics, 37, 935–964. https://doi.org/10.1002/2017TC004792.

Péron-Pinvidic, G., Manatschal, G., Osmundsen, P.T., 2013. Structural comparison of archetypal Atlantic rifted margins: a review of observations and concepts. Marine and Petroleum Geology. 43, 21–47. http://dx.doi.org/10.1016/j.marpetgeo.2013.02.002.

Pinxian Wang, Chi-Yue Huang, Jian Lin, Zhimin Jian, Zhen Sun, Minghui Zhao, The South China Sea is not a mini-Atlantic: plate-edge rifting vs intra-plate rifting, National Science Review, Volume 6, Issue 5, September 2019, Pages 902–913.

Pubellier, M., Morley, C., 2014. The Basins of Sundaland (SE Asia); evolution and boundary conditions. In: Pubellier, M., McIntosh, K., Franke, D., Li, C.F., Menier, D. (Eds.), Marine and Petrol, "Evolution, Structure, and Sedimentary Record of the South China Sea and Adjacent Basins". Geology Special Publication.

Qing Ye, Lianfu Mei, Hesheng Shi, Giovanni Camanni, Yu Shu, Jing Wu, Lu Yu, Peng Deng, Gang Li, 2018. The Late Cretaceous tectonic evolution of the South China Sea area: An overview, and new perspectives from 3D seismic reflection data. Earth-Science Reviews, 187, 186-204. https://doi.org/10.1016/j.earscirev.2018.09.013.

Replumaz, A., Tapponnier, P., 2003. Reconstruction of the deformed collision zone between India and Asia by backward motion of lithospheric blocks. Journal of Geophysical Research. 108 (B6), 2285.

Reynir Fjalar Reynisson. Deep structure and sub-basalt exploration of the mid-Norwegian margin with emphasis on the Møre margin. Doctoral dissertation, Norwegian University of Science and Technology, Trondheim, Norway, October 2010.

R. Mjelde, T. Raum, A. Kandilarov, Y. Murai, T. Takanami, 2009. Crustal structure and evolution of the outer Møre Margin, NE Atlantic, Tectonophysics, 468, 224-243.

Roberts, D., 2003. The Scandinavian Caledonides: event chronology, palaeogeographic settings and likely modern analogues, Tectonophysics, 365, 283-299.

Simon Gozzard, Nick Kusznir, Dieter Franke, Andrew Cullen, Paul Reemst, Gijs Henstra, 2018. South China Sea crustal thickness and oceanic lithosphere distribution from satellite gravity inversion. Petroleum Geoscience, 25, 112-128.

Scrutton, R. A., Stoker, M. S., Shimmield, G. B. & Tudlope, A. W, 1995. The tectonics, sedimentation and stratigraphy of the North Atlantic Region. Geological Society, London, Special Publications, 90, 1-28.

Zhichao Zhou, Lianfu Mei, Jun Liu, Jinyun Zheng, Liang Chen, Shihao Hao, 2018. Continentward-dipping detachment fault system and asymmetric rift structure of the Baiyun Sag, northern South China Sea, Tectonophysics, 726, 121-136.

[1]https://factmaps.npd.no/factmaps/3_

[2]https://factpages.npd.no/en/wellbore